ACCURACY ANALYSES OF NUMERIC WEATHER PREDICTION-BASED STRATIFORM AND CONVECTIVE PRECIPITATION SHORT-TERM FORECASTS OVER TURKEY

A THESIS SUBMITTED TO
THE GRADUATE SCHOOL OF NATURAL AND APPLIED SCIENCES
OF
MIDDLE EAST TECHNICAL UNIVERSITY

BY

BERİL AYDIN

IN PARTIAL FULFILLMENT OF THE REQUIREMENTS
FOR
THE DEGREE OF MASTER OF SCIENCE
IN
CIVIL ENGINEERING

JANUARY 2023

Approval of the thesis:

ACCURACY ANALYSES OF NUMERIC WEATHER PREDICTION-BASED STRATIFORM AND CONVECTIVE PRECIPITATION SHORT-TERM FORECASTS OVER TURKEY

submitted by **Beril Aydın** in partial fulfillment of the requirements for the degree of **Master of Science** i**n Civil Engineering, Middle East Technical University** by,

Prof. Dr. Halil Kalıpçılar
Dean, Graduate School of **Natural and Applied Sciences** _____

Prof. Dr. Erdem Canbay
Head of the Department, **Civil Engineering** _____

Prof. Dr. İsmail Yücel
Supervisor, **Civil Engineering, METU** _____

Assoc. Prof. Dr. M. Tuğrul Yılmaz
Co-Supervisor, **Civil Engineering, METU** _____

Examining Committee Members:

Assoc. Prof. Dr. Ali Ercan
Civil Engineering, METU _____

Prof. Dr. İsmail Yücel
Civil Engineering, METU _____

Assoc. Prof. Dr. M. Tuğrul Yılmaz
Civil Engineering, METU _____

Assoc. Prof. Dr. Koray K. Yılmaz
Geological Engineering, METU. _____

Assoc. Prof. Dr. Sertaç Oruç
Civil Engineering., Kırşehir Ahi Evran Uni. _____

Date: 18.01.2023

I hereby declare that all information in this document has been obtained and presented in accordance with academic rules and ethical conduct. I also declare that, as required by these rules and conduct, I have fully cited and referenced all material and results that are not original to this work.

Name Last name : Beril Aydın

Signature :

ABSTRACT

ACCURACY ANALYSES OF NUMERIC WEATHER PREDICTION-BASED STRATIFORM AND CONVECTIVE PRECIPITATION SHORT-TERM FORECASTS OVER TURKEY

Aydın, Beril
Master of Science, Civil Engineering
Supervisor: Prof. Dr. İsmail Yücel
Co-Supervisor: Assoc. Prof. Dr. M. Tuğrul Yılmaz

January 2023, 93 pages

This study was carried out to determine whether convective and stratiform (large-scale) precipitation datasets obtained from 5 model forecast-based products would be an adequate alternative for regions where station-based observation networks are sparse. Verification of precipitation types (convective or stratified) from numerical weather forecast (NWP) models (ALARO, CFS, ECMWF HRES, GFS, WRF) is done using station-based observations. Statistical assessments between these precipitation types in different topographies (complex and non-complex) are available between 2015 and 2018. Reference data are obtained from 836 Automatic Observation Stations (OMGI) operated by the Turkish State Meteorological Service (TSMS). Accuracy assessments are reviewed separately for each precipitation type (total, convective, stratiform) and topography (entire area, complex regions, non-complex regions). The results show that all model products have an average correlation of 0.6 in total and large-scale precipitation for all areas. In contrast, the convective component of precipitation has an average correlation of 0.16 and 0.19 for complex and non-complex regions, respectively. In complex areas where the risk of flash flooding is high and the slope is more than 5% under the influence of convective precipitation, the low prediction performance of model products reduces

the ability to take precautions for dangerous situations. Overall, the ECMWF HRES product has the highest accuracy in total precipitation for all areas, while the WRF product has the highest correlation coefficient and closest spatial distributions in all regions for convective precipitation. The findings of this study will assist the global literature examining regions with complex topography not only over the entire study area but for future hydrological and hydrometeorological studies.

Keywords: Complex Topography, Numerical Weather Prediction, Convective Precipitation, Stratiform Precipitation, Accuracy Assessments

ÖZ

TÜRKİYE ÜZERİNDE KONVEKTİF VE CEPHESEL YAĞIŞ TAHMİNİNDE MODEL-TABANLI KISA VADELİ YAĞIŞ TAHMİNLERİNİN DOĞRULUK DEĞERLENDİRMESİ

Aydın, Beril
Yüksek Lisans, İnşaat Mühendisliği
Tez Yöneticisi: Prof. Dr. İsmail Yücel
Ortak Tez Yöneticisi: Doç. Dr. M. Tuğrul Yılmaz

Ocak 2023, 93 sayfa

Bu çalışma, tahmine dayalı 5 model üründen elde edilen konvektif ve stratiform (büyük ölçekli) yağış veri setlerinin, istasyon tabanlı gözlem ağlarının seyrek olduğu bölgeler için yeterli bir alternatif olup olmayacağını belirlemek amacıyla yapılmıştır. Sayısal hava tahmini (NWP) modellerinden (ALARO, CFS, ECMWF HRES, GFS, WRF) yağış türlerinin (konvektif veya cephesel) doğrulanması, istasyon tabanlı gözlemler kullanılarak yapılır. Farklı topografyalardaki (karmaşık ve karmaşık olmayan) bu yağış türleri arasındaki istatistiksel değerlendirmeler 2015 ile 2018 yılları arasında mevcuttur. Referans veriler, Meteoroloji Genel Müdürlüğü (MGM) tarafından işletilen 836 Otomatik Gözlem İstasyonundan (OMGI) elde edilmektedir. Doğruluk değerlendirmeleri, her yağış türü (toplam, konvektif, cephesel) ve topografya (tüm alan, karmaşık bölgeler, karmaşık olmayan bölgeler) için ayrı ayrı incelenir. Sonuçlar, tüm model ürünlerin toplam ve tüm alanlar için cephesel yağışta ortalama 0.6 korelasyona sahip olduğunu göstermektedir. Buna karşılık, yağışın konvektif bileşeni, karmaşık ve karmaşık olmayan bölgeler için sırasıyla 0.16 ve 0.19'luk bir ortalama korelasyona sahiptir. Ani sel riskinin yüksek olduğu ve konvektif yağış etkisinde eğimin %5'ten fazla olduğu karmaşık alanlarda, model

ürünlerin düşük tahmin performansı, tehlikeli durumlar için önlem alma yeteneğini azaltır. ECMWF HRES ürünü, tüm alanlar için toplam yağışta en yüksek doğruluğa sahipken, WRF ürünü, konvektif yağış için tüm bölgelerde en yüksek korelasyon katsayısına ve en yakın mekansal dağılımlara sahiptir. Bu çalışmanın bulguları, sadece tüm çalışma alanı üzerinde değil, aynı zamanda gelecekteki hidrolojik ve hidrometeorolojik çalışmalar için karmaşık topografyaya sahip bölgeleri inceleyen küresel literatüre yardımcı olacaktır.

Anahtar Kelimeler: Karmaşık Topografya, Sayısal Hava Tahmini, Konvektif Yağış, Cephesel Yağış, Doğruluk Değerlendirmeleri

To my family,

ACKNOWLEDGEMENTS

First and foremost, I would like to express my sincere gratitude to my advisor Prof. Dr. İsmail Yücel, for his patience, continuous support, and immense knowledge. Throughout my M.S. study, he always encouraged me with his calmness and sincerity. With the same feelings, I would also like to express my sincere thanks to my co-advisor, Assoc. Prof. Dr. M. Tuğrul Yılmaz. His wisdom, plentiful experiences and advice carried me through all the stages, as he was only a phone call away during this study.

I would like to express my special thanks to Dr. Muhammed Amjad. Although he was not with me physically, he made me feel he was always with me with his patience and knowledge, who always shed light on my path while laying the foundation of everything I know in this work.

I would also like to thank my office mates Dr. Eren Düzenli, Dr. Burak Bulut, Dr. Mehdi Afshar, Ali Serkan Bayar, Ali Cem Çatal and Çağatay Çakan for being there for me whenever I needed them and being not only office mates but real friends. I am grateful to them for proving that we can always come across as good, honest, and generous people with shared values in life.

I want to thank my companions, Gizem Genç and Ceren Durğut, for being with me and supporting me every minute of my higher education life. I believe we will always keep walking together after this road that we started and finished together.

Finally, but most importantly, I would like to thank my dear family for never leaving my hand on this path and always being behind me. I would like to thank my mother, Gönül Aydın, who I always take as an example with her guidance; my father, Kemal Aydın, who can make me laugh in my most desperate times; my sister Sevil Aydın, who always comes out when I need her the most. To my family, I give everything, including this thesis.

TABLE OF CONTENTS

LIST OF TABLES

TABLES

LIST OF FIGURES

FIGURES

LIST OF ABBREVIATIONS

ABBREVIATIONS

TSMS	Turkish State Meteorological Service
ECMWF	European Center of Medium-range Weather Forecast
NCEP	National Service for Environmental Prediction
NCAR	National Center for Atmospheric Research
HRES	High Resolution
ALADIN	Aire Limitée Adaptation Dynamique Développement International
AROME	Application of Research to Operations at Mesoscale
ALARO	ALadin AROme
WRF	Weather Research and Forecasting Model
GFS	Global Forecast System
CFS	Climate Forecast System
IFS	Integrated Forecasting System
ARPEGE	Action de Recherche Petite Echelle Grande Echelle
3MT	Modular Multiscale Microphysics and Transport
MARS	Meteorological Archival and Retrieval System
MMM	Mesoscale and Microscale Meteorology Laboratory
NOAA	National Center for Oceanic and Atmospheric Research
AFWA	Air Force Weather Agency

FAA	Federal Aviation Administration
ARW	Advanced Research WRF
NMM	Non-hydrostatic Mesoscale Model
TP	Total Precipitation
CP	Convective Precipitation
LSP	Large-scale Precipitation
SD	Standard Deviation
ErrSD	Error Standard Deviation
RMSE	Root Mean Square Error
CC	Correlation Coefficient
SNR	Signal to Noise Ratio
CPI	Categorical Performance Indices
POD	Probability of Detection
FAR	False Alarm Ratio
CSI	Critical Success Index
PC	Percent Correct

CHAPTER 1

INTRODUCTION

1.1 Motivation

Water is one of the most fundamental components of the Earth's climate. Today, sustainable water resources management is one of the most critical issues in the whole world. The amount of precipitation determines the amount of drinking water, irrigation, and hydropower plants (Zahedi et al., 2022). Precipitation affects all areas of daily human life, from residential areas to tourism, from transportation to agriculture (Jodar-Abellan et al., 2019). Besides, there are extreme precipitation events that may result in flash floods or landslides which are direct threats to all living things (Talchabhadel et al., 2022). These extreme events can also affect by various factors, such as topographical complexity (L. Yu et al., 2020). For these reasons, it is essential to make precipitation forecasts accurately.

Unknown future precipitation amounts make it difficult to take precautions against losses. Spatio-temporal alterations of precipitation have caused more undesired hazards in recent decades and show different patterns in global, continental and regional scales (IPCC, 2014; Mathew et al., 2021). Numerical weather prediction (NWP) models with different scales, established in many NWP centers to carry through short-term weather forecasts (Ren et al., 2022). These NWP models are an alternative to predicting precipitation components in regions with complex topography where meteorological stations are sparse (Amjad et al., 2020). The accuracy of the NWP models is related to the horizontal resolution and physical parametrization. Moreover, this accuracy is also limited with initial and boundary conditions such as temperature, pressure, moisture or solar radiation and their domains (Bližňák et al., 2017). With technology-advancing computational techniques, NWP models can fulfill the needs for precipitation forecasts. Worldwide

studies have been and are being conducted to evaluate the dependability of these NWP models in predicting precipitation (Amjad et al., 2020; Saedi et al., 2020; Singhal et al., 2022a; Sokol et al., 2022). Some of the NWP models with various spatial and temporal resolutions obtained from different centers are European Centre for Medium-Range Weather Forecasts (ECMWF), ECMWF-High Resolution (ECMWF HRES) (Singhal et al., 2022b), ALADIN (Aire Limitée Adaptation Dynamique Développement International)-AROME (Application of Research to Operations at Mesoscale) (ALARO) (De Troch et al., 2013), Weather Research and Forecasting Model (WRF) (Duzenli et al., 2021), Global Forecast System (GFS) (Ashrit et al., 2020; Rao et al., 2022; Sridevi et al., 2020) and The Climate Forecast System (CFS) (Hazra et al., 2016). Hydrological studies require reliable precipitation predictions since the point form station observations lack the information.

While the NWP models are used to reduce the uncertainties in estimating, the accuracy of these models has great importance since these uncertainties impact whole hydrometeorological calculations (Edouard et al., 2018). One of the main reasons for these uncertainties is whether the topography in the indicated area is complex. Topography may be one of the most substantial of these because the topography and precipitation relationship is not just about height change; there are local interactions such as air pressure, slope or slope direction (Li et al., 2021). These kinds of perilous weather events, which develop depending on many parameters (Guo et al., 2021; Špitalar et al., 2014), make it difficult for the models to make accurate predictions, as the numerical precipitation amount is not homogeneously spread over the complex topographies (Roberts, 2008). Extreme precipitation estimation with exact location and intensity is vital since floods happen rapidly in mountainous regions in such complex topographies.

The existence of precipitation components with different obvious cloud microphysical properties has been known for a long time (Kirsch et al., 2019). The convective component of precipitation is at the forefront in the formation of flash floods that increase the severity of events associated with deep convective clouds (Llasat et al., 2016). Convection has a principal role in cloud formation that

designates the intensity and impact of the precipitation, which comprises a rapid increase in warmed air in heavy rainfalls (Zeng et al., 2021). While such precipitation has high intensities in small areas, stratiform precipitation plays a significant role in natural water cycles with low precipitation intensity in large areas. In addition to the importance of the total precipitation forecast, the correct estimation of the precipitation components affects many areas in terms of social and economic aspects. Differentiation of convective and stratiform precipitation in regions with complex topography and evaluation of the performance of numerical weather forecast models allows many hydrological studies to be carried out.

1.2 Literature Review

While investigation of the precipitation accuracy is widely performed (Akinyemi et al., 2020; Chen et al., 2021; Jafarpour et al., 2022; Jiang et al., 2021; C. Yu et al., 2020; Zhang et al., 2022; Z. Zhang et al., 2019), the number of studies investigated the performance over complex topography is much less (Amjad et al., 2020; Lei et al., 2021; Ward et al., 2011; L. Yu et al., 2020). On the other hand, there are only a few studies explicitely investigated the accuracy of convective and stratiform components of the precipitation products (Feloni et al., 2019; Kyselý et al., 2016; Wang et al., 2021). Past studies focused on flat regions (Bližňák et al., 2019; Šaur et al., 2021; Yang et al., 2019). However, not many studies intercompared the accuracy of convective and stratiform precipitation using different NWP models over complex topographies (Amjad et al., 2020; Duzenli et al., 2020; Foth et al., 2021; Sahlaoui et al., 2020; Yucel and Onen, 2014; Zhao et al., 2021).

This study intercompared the accuracy of 5 NWP model forecasts (ALARO, ECWMF, GFS, CFS, WRF) over a complex region in Turkey. The data used in the study are evaluated for the first time regarding the number of models, study time, and study area. Analyses are performed over Turkey for three different precipitation types (total, convective, and large-scale) concerning observation data from 836 measuring stations. Evaluation studies for total, convective, and large-scale

precipitation include precipitation statistics, error precipitation statistics, precipitation frequency analyses, categorical performance indices and spatial distributions to compare the models' performances in complex and non-complex areas.

The data used in the study are evaluated for the first time regarding the number of models, study duration, and study area. This study reveals many original and new results for our country and the literature with the following items.

1) In our country, the precipitation data obtained over the whole country is divided into two convective and stratiform and separately evaluated using different weather forecast models and ground observation data.

2) High-resolution convective and stratiform precipitation forecasts from ECMWF (HRES), ALARO, WRF, GFS, and CFS presented in Turkey have been comparatively evaluated over Turkey.

3) Extensive analyses of model-based assessment of precipitation products over complex topography have been performed.

4) The temporal and spatial variation of the uncertainty of both convective and stratiform precipitation of different models in different regions of Turkey has been demonstrated.

5) In which regions of our country is there more convective and stratiform precipitation and the rates of these precipitations have been investigated numerically. This study reveals the percentage of convective precipitation in all precipitation and its spatial distribution with ground observation data and models.

The results of this study will contribute in many ways to the ongoing and future studies in various fields that need precipitation data and will prepare the ground for them. The importance of this study is that it analyzes the model-based accuracies of precipitation components throughout Turkey.

CHAPTER 2

METHODOLOGY

Accuracy analyzes are carried out between 5 different NWP models and ground observation stations used as references in this study, which is carried out on an area with a complex topography such as Turkey.

Different features of NWP models such as parameterization, resolution or sensitivity, cause different estimation results. In this context, accuracy analysis has a great essence. As shown in Figure 2.1, precipitation statistics, categorical performance indices are calculated for more detailed interpretation, intensity-frequency relations are discussed and their spatial distribution maps are examined. Finally, these results are compared at various time scales.

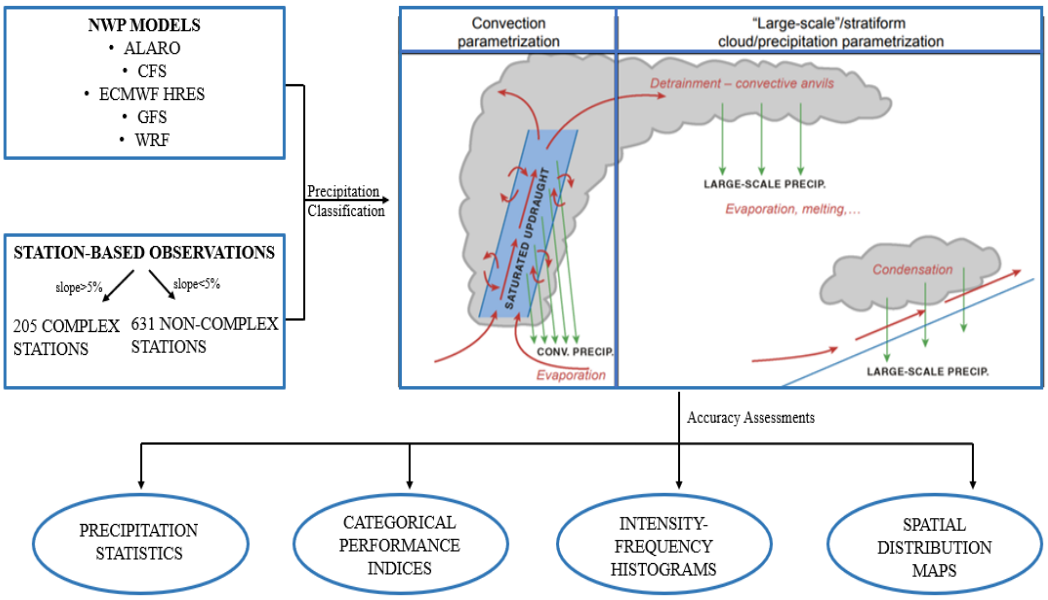

Figure 2.1. Flow chart of the study

2.1 Study Area

The study area is selected as entire Turkey that is widely known for its complex topography with a mean elevation of 1132 m, where it has a surface area of 783,562 km^2 (Amjad et al., 2020; Bostan et al., 2012). It is located in the Eastern Mediterranean region with an annual average precipitation of 573.4 mm (Turkish State Meteorological Service (TSMS), 2020). Latitude and longitude coordinates are 35-43 and 25-45, respectively. Due to its coasts to the Mediterranean, Black Sea, and the Aegean Sea, more than one climate type is observed all year round. The effect of greenery and topography on the existence of diverse climatic conditions is relatively high (Amjad et al., 2020). While the mild climate is dominant in the coastal regions, the summers are hot and dry in the interior regions and the winters are cold (Sensoy et al., 2008). The Black Sea coast has the highest rainfall rate throughout the year, known for its Oceanic climate, as it receives precipitation at all times of the year. Primarily the eastern part of the Black Sea receives the most precipitation in the country, with an annual 820-2300 mm (TSMS, 2018). This amount of precipitation falls below 400 mm per year in the driest regions of the central area (TSMS, 2018). Mountains may induce such differences by acting as barriers. Since mountains cut the wind suddenly, the orographic effect is prevalent and determines the amount of precipitation rate (Gottardi et al., 2012). For example, the Hopa region in Artvin, one of the study area's rainiest districts, is located in the coastal area without being affected by the mountain blockage. However, Bayburt station, located in the same region's interior, receives almost one-fifth of the Hopa. The most rugged and mountainous regions are located mainly on the eastern side. In addition, there are some principal areas with complex topographies on the other sides: the Northern Anatolian Mountains, where the mountains are parallel to the sea and the Taurus Mountains in the south. Local topographical variations show its effect dominantly in complex parts since these regions demonstrate high sensitivity microphysical cloud processes that affect the formation of convective precipitation (Gao et al., 2018). In addition to this formation, as the air warms up, the rising air moves parallel to the

slope, causing the moisture to condense and fall. Therefore, the diversity of the topography affects the distribution of precipitation; as the slope increases, the amount of precipitation increases (Hughes et al., 2009). Moreover, the opportunities are limited while measuring precipitation using ground observation stations with high accuracy where the topographic conditions are not favorable. Since the placing and installing of these stations are laborious in such rough terrains due to sparseness. For this reason, it is crucial to compare the NWP models in such places and evaluate their performances to increase the dependability in hydrological studies. Furthermore, it would not be correct to directly relate the complexity of the topography with the elevation because a region may have a flat surface even though it has a high elevation (Elibüyük and Yılmaz, 2010; Seastedt et al., 2004). In this study, the term complex refers to places with more than a 5 percent slope, even if the elevation is low. If the change in slope per unit distance is more than 5 percent, it is classified as a complex region. Otherwise, it is classified as a non-complex region (Amjad et al., 2020).

2.2 Datasets

The performances of the five model-based precipitation products (ALARO, CFS, ECMWF, GFS, WRF) are evaluated by taking the ground observation stations (836 in total) data as the reference dataset.

2.2.1 Ground-based gauge precipitation data

Receiving meteorological data such as precipitation in Turkey, which has a very complex topography, is a very laborious task due to the difficulty of station installation. Such problems also increase the importance of model-based precipitation forecasts. The most dependable measurements to be used in the validation of model-based datasets are again at ground source measurement stations

and this method is correspondingly widely used in the literature (Amjad et al., 2020; Bağçaci et al., 2021; Chen et al., 2018).

In this study, we performed accuracy analyses on complex and non-complex areas for the two precipitation components. In contrast to earlier studies, this study seeks to overcome the effect of topography in precipitation estimations intercompared with five different NWP models. In previous approaches, there are different convective and stratiform precipitation separation methods. Precipitation texture algorithm (Churchill and Houze Jr, 1984), vertical wind speed (Poujol et al., 2020), intensity and sharpness of the maximum horizontal models of radar reflectivity (Steiner et al., 1995), raindrop size distribution measured by a disdrometer (Das and Maitra, 2018; Foth et al., 2021; Ghada et al., 2019; Seela et al., 2018; A. Zhang et al., 2019), precipitation intensity and lightning (Chen et al., 2020; Gaal et al., 2014; Xu et al., 2014), determining a width threshold for the convective zone (Caniaux et al., 1994) and setting a specific threshold (Churchill and Houze Jr, 1984; Dutton and Dougherty, 1979; Llasat et al., 2016; Watson and Holle, 1982; Xu et al., 1995). Among these methods, determining a specific threshold value according to the precipitation intensity is the most consistent regarding applicability to ground observation stations. According to this method, precipitation is classified as convective if it has an intensity above the determined value and stratified if not. Applying the determined threshold value in different topographies provides convenience for comparison because there are no other parameters to be considered while making this classification. These data are obtained from the Turkish State Meteorological Service (TSMS). The total number of stations is 836 after the quality control process. These stations are classified according to a five percent slope; 205 are in the complex and the remaining 631 are in the non-complex topography area. The available data is on a daily and hourly time scale and covers four years, from 2015 to 2018.

2.2.2 Model-based precipitation data

NWP models use mathematical formulas based on physical principles of atmospheres and oceans to estimate weather conditions. They use a group of governing equations such as conservation of momentum, conservation of mass, conservation of energy, or ideal gas law to determine the flow of fluids. Afterwards, these equations are translated into computer codes combined with initial and boundary conditions. Many models operated by several countries in global or regional domains using instant weather conditions. The need for higher-resolution regional models increases due to global models' relatively low horizontal and vertical resolutions. These NWP models produce short-term weather predictions or long-term climate projections. The forecast ability of these models depends on the intensity and quality of observations used as inputs and they require powerful supercomputers as they are computationally expensive. Uncertainties due to the chaotic nature of the atmosphere, initial and boundary conditions or physical parameters affect the quantitative predictions of NWP models (Koukoula et al., 2019). Some meteorological events are microscopic scale or complicated. Each process cannot be directly estimated; parametrization is required based on physical and statistical expressions. So, almost every step contains estimations and approximations. Figure 2.2 depicts some of the parameters and physical processes. Hence, parameterization becomes a part of it because models cannot be clearly estimated in detail in forecast equations.

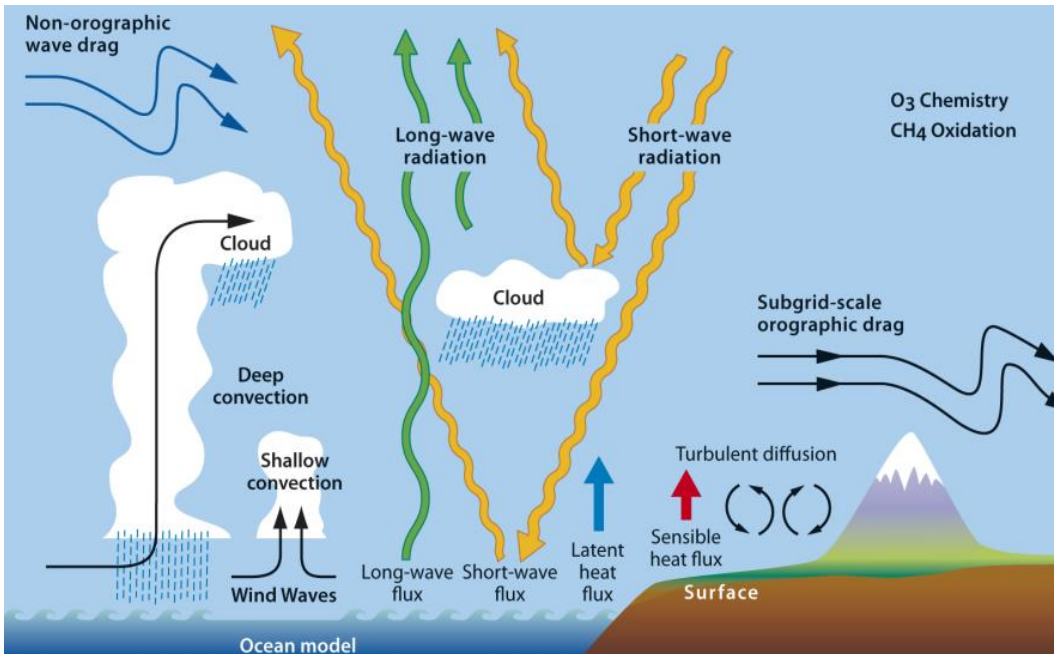

Figure 2.2. Physical parametrized processes in a NWP model (ECMWF, 2020)

This study uses five NWP model products: ALARO, CFS, ECMWF HRES, GFS, and WRF. Physical processes in the atmosphere are shown in NWP models with a series of parametrization (McTaggart-Cowan et al., 2019). Each model uses different numerical solutions with different sensitivities, so, they have distinctive predictions. ALARO, ECMWF, and WRF models' Turkey domain as seen in Figure 2.3. Regional models may have finer grid spacing and less computational effort.

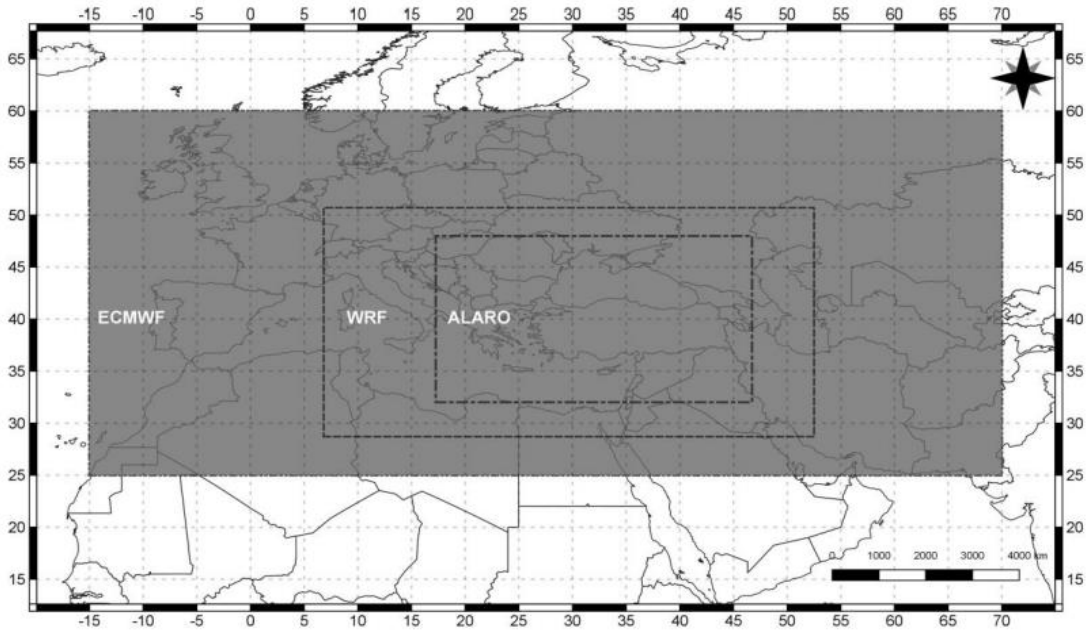

Figure 2.3. ALARO, ECMWF and WRF precipitation products domains (Aksoy, 2020)

2.2.2.1 ALARO

AROME (Applications of Research to Operations at Mesoscale) software is a small-scale Digital Weather Forecast model run by Meteo-France in 2008. Since AROME software is costly in real-time weather forecast calculation, the ALARO (ALadin-AROme) model is based on the French-origin Aire Limitée Adaptation Dynamique Development International (ALADIN) model has been developed with 10 km resolution (Simon et al., 2021). The AROME model has 2.5 km inter-scale resolution and mesoscale convection, which has a limited area and is used for fine modeling (Yessad, 2013). ALARO is a version of ALADIN used in several central and eastern European countries. The ALARO model has horizontal a resolution of 4.5 km and has 60 vertical layers. The parameterization of the ALARO model is projected to run at a resolution prone to convection generation. In the last decade, a physical parameterization scheme named 3MT (Modular Multiscale Microphysics and Transport) has been developed. It is based on a parameterization of deep and shallow

convection (Giot et al., 2015). Several countries have used and tested for regional studies (Top et al., 2021) and other parameterization schemes were also carried out in accordance with 3MT. Boundary conditions are obtained in global ARPEGE (Small-Scale Large-Scale Research Action, Action de Recherche Petite Echelle Grande Echelle) at 3-hour intervals. ARPEGE model is used in Meteo-France and ECMWF. At ECMWF, it is called IFS (Integrated Forecast System). A limited space version of the ARPEGE global model opened in 1990 covers the countries of Bulgaria, Hungary, Czech Republic, Poland, Romania and Slovakia. Algeria, Belgium, Morocco, Tunisia, Portugal, Austria, Croatia, Slovenia and Turkey were included in the next period. (Karadavut, 2014). ALARO model is operated four times daily (00, 06, 12, and 18 UTC) in TSMS. The datasets of the ALARO model are obtained from the TSMS.

2.2.2.2 CFS

Provided by the United States National Centers for Environmental Prediction (NCEP) in 2004, CFS is a model that reflects the interaction between Earth's atmosphere, lands, oceans, and seas to act as a bridge between weather and climate. The CFS model used in this study with a spatial resolution of 0.5° is used to analyze, reanalyze and predict precipitation data. This model is lower-resolution version of GFS. The model is called CFSv1 between 2004-2011 and CFSv2 after 2011, the enhanced quality of version It is a fully-coupled global climate model that makes past, present and future climates with high-performance computers (Saha et al., 2006). Convective parameterization uses simplified Arakawa-Schubert convection. The CFS model has a 4-layer NOAH land surface model and a two-layer dynamic sea ice model. It implements mountain blockage and orographic gravitational wave resistance at sub-grid scale. CFS scientifically combines data from many sources such as ground observations, air balloon observations, satellite and aircraft (NCEP, 2022). This model is initialized four times per day (00, 06, 12, and 18 UTC). In this study, 1-daily accumulated which is derived from 6-hourly total and convective

precipitation is obtained from NCAR archive. Large-scale precipitation is procured from subtracting convective precipitation from total precipitation.

2.2.2.3 ECMWF HRES

ECMWF is a weather forecasting model used for atmospheric research purposes established in 1975 with 13 countries and requires 4DVAR (4-dimensional variation data assimilation system) to be started (ECMWF, n.d.). It is supported by most of the countries in Europe, Turkey became a member of ECMWF in 1976. ECMWF provides hydrological estimations, air quality analysis, climate monitoring, ocean circulation analysis, global numerical weather predictions, and atmospheric composition monitoring. Also, the center plays a crucial role in developing data assimilation and modeling systems. Thus, it improves the accuracy of model forecasting. The products presented from the medium-term forecasts have a spatial resolution of 2.5°, while the dataset used in this study has a spatial resolution of 0.1°. While ECMWF estimates 52 ensemble members separately based on IFS created twice a day, one of these members has a higher resolution than the others and is called HRES in ECMWF (Yang et al., 2022). The initial conditions of ECMWF HRES are the most accurate prediction of instant state and use the best description of model physical parameters. These products make separate forecasts for the convective and large-scale components of the precipitation and the total precipitation forecast. The cloud scheme describes the large-scale precipitation and the convection scheme in the IFS generates the convective precipitation (ECMWF, 2022). In this study, 1-daily accumulated precipitations from deterministic forecast are used. The datasets are obtained from the Meteorological Archival and Retrieval System (MARS) of ECMWF.

2.2.2.4 GFS

The GFS model used in this study, produced by the National Centers for Environmental Prediction (NCEP) and started operating in 2015, is obtained from the National Atmospheric Research Center (NCAR) with a resolution of 0.25°, covering the entire globe. The GFS model can be run at different spectral resolutions on a hybrid sigma/pressure coordinate (Lien et al., 2016). It is one of the most advanced NWP models in the world. A weather prediction model generates data for many atmospheric and land-soil variables—for instance, soil moisture, wind, precipitation, or temperature (NCEP, 2022). The system combines four models (sea ice, atmosphere, ocean, and land) to get accurate weather predictions. However, it does not take into account the topography near water bodies, resulting in poor accuracy in these areas. In the 2015s, the system was upgraded with new supercomputers 2017 after failing to predict Hurricane Sandy and lagging behind other models. Regular changes are still made to improve the estimation performance of the GFS model. It is a constantly evolving weather model. The model is run four times a day and produces predictions up to 16 days. As any numerical model, forecast skill decreases with time, only larger scale forecasts can remain with high accuracy. In this study, 1-daily accumulated, which is derived from the 6-hourly total, convective and large-scale precipitation, is obtained from NCAR archive.

2.2.2.5 WRF

The WRF model, run by the Mesoscale and Microscale Meteorology Laboratory (MMM) within the National Center for Atmospheric Research (NCAR). It produces simulations based on observations and analysis, that is, real conditions or idealized conditions. Since the state-of-art WRF model is open-source and has compressible equations which are Eulerian, non-hydrostatic. The model is designed for operational forecasting and atmospheric research since it serves wide range of meteorological applications. It can be developed by many users and can be used in many

atmospheric research centers such as universities and institutes. WRF simulations are based on actual atmospheric conditions, serving a variety of meteorological studies at many scales ranging from few meters to thousands of kilometers. It can be used in a resolution of 1-10 km. It is suitable for use in many fields such as research and operational numerical weather prediction, data-assimilation, parameterized-physics research, downscaling climate simulations, driving air quality models and ideal simulations (Jain, 2015). The model can be operated in two ways: ARW (Advanced Research WRF) developed by NCAR and NMM (Non-hydrostatic Mesoscale Model). The ARW solver uses a vertical coordinate system that follows the change of terrain structure based on topography; NMM was developed for operational use. However, there are no significant differences between dynamic solvers. Collaborators of the model include the National Center for Oceanic and Atmospheric Research (NOAA), the Air Force Weather Agency (AFWA), the Naval Research Laboratory, the University of Oklahoma, and the FAA (Federal Aviation Administration) (NCAR, 2022). The WRF modeling system is successful in predicting heavy precipitation over complex terrains and medium-sized convective systems in several regions (Yucel et al., 2015) .The WRF datasets used in this study are obtained from TSMS with a spatial resolution of approximately 4 km and updated for six hours (00, 06, 12, and 18 UTC).

2.2.3 Study Period

Table 2.1 shows the informations about the datasets used. Due to different availability conditions, the possible common period that can be used in the study is determined as 2015-2018 for daily scale, 2015-2020 for hourly scale.

Table 2.1. Information about the datasets used in this study

Sr. No	Dataset	Spatial Resolution	Temporal Resolution	Period	Source
1	Observation	-	Daily Hourly	2003-2020	TSMS
2	ALARO	~0.045^{o}	Daily	2011-2018	TSMS
3	CFS	0.5°	Daily Hourly	2013-2020	NCEP, NCAR Archive
4	ECMWF HRES	0.1°	Daily Hourly	2007-2020	ECMWF MARS Archive
5	GFS	0.25°	Daily Hourly	2015-2020	NCEP, NCAR Archive
6	WRF	~0.040^{o}	Daily	2013-2018	TSMS

2.3 Pre-processing of Data

2.3.1 Gridded Data to Point Data Conversion

This study's reference data measured from ground observation stations are in point form. As the examples are widely seen in the literature, the model data are also converted from gridded to point forms (Amjad et al., 2020; El Kenawy et al., 2015). Due to the inadequate number of ground-based stations in Turkey, the opposite path

could not be followed, which is point data to gridded data conversion. Point form model products are obtained by selecting the closest station to the existing grid center.

2.3.2 Quality Control Process

Automatic Meteorology Observation Stations (OMGI), which started to be established in Turkey in the 2000s and whose number is increasing day by day, have sometimes been replaced with manual measurement stations. They have gained function by being established in regions without a station. Obtaining meteorological data such as precipitation in Turkey, which has a very complex topography, is a very laborious task due to the difficulty of station installation. Such problems again increase the prominence of model-based precipitation forecasts. Again, the most reliable measurements to validate model-based datasets are at ground-based measurement stations. This method is also widely used in the literature, and in this study, it is obtained by comparing the precipitation error statistics with the reference data. The ground observation station data used in this study are obtained from the TSMS. Today, there are more than 2000 stations, and only about 10 percent are measured manually.

The minutely raw data obtained from TSMS are subjected to quality control due to lack of data, inconsistency, and discontinuance. This quality control process filter values greater than the maximum precipitation values given by TSMS for various periods. These values are determined as 50.5 mm/5min, 131 mm/hour and 490 mm/day. Afterward, stations are filtered according to monthly mean, standard deviation and long-term mean criteria. These are common simple methods to reduce noise in the datasets. At the end of this filtering process, the hourly and daily precipitation data of the remaining 836 ground observation stations between 2003 and 2020 are taken as reference and these datasets are used in the evaluations (Figure 2.4). In line with this method, all the precipitation data are extracted for 5 model predictions from gridded data covering the location of 836 observation stations. As

a result, a total of 6 datasets, including observation, are made ready for analysis.

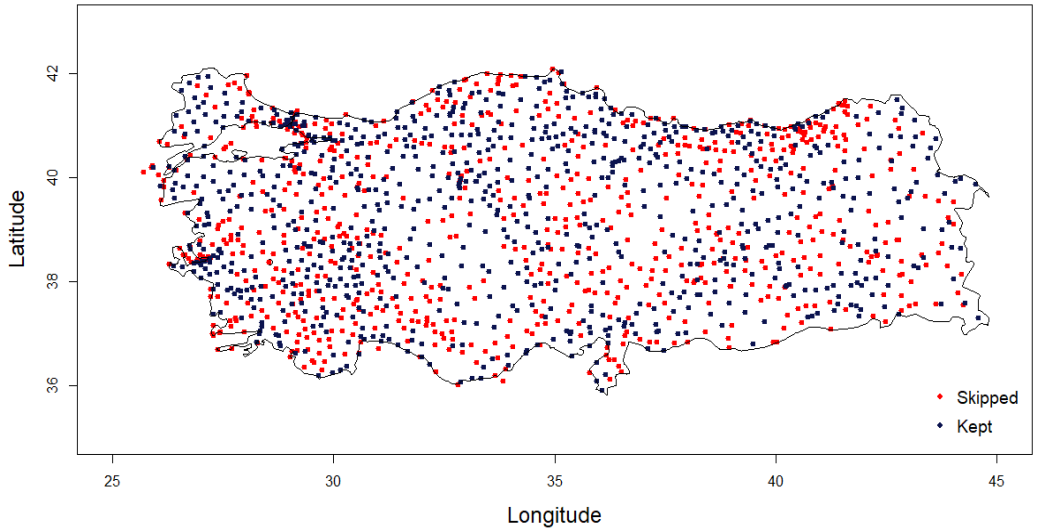

Figure 2.4. Locations of total kept and skipped stations in Turkey

2.3.3 Classification of Stations as Complex or non-Complex

The varying topography has a massive impact on climate. Topographical diversity may create microclimates by causing different winds, rain and snowfall. It is necessary to understand the spatial pattern and effect of topography in regions where the station density is low. Meteorological station data should be supported by other information to assess the precipitation amount and understand the impact of topographical complexity (Johansson and Chen, 2003).

In this study, complex and non-complex classification is made according to the percent slope of 836 stations located in the study area. The stations are divided into 2 classes, with a threshold slope value of 5 percent, as complex above 5 percent and as non-complex, those below 5 percent (This threshold is selected based on the study of Amjad et al., 2020). The distributions of complex and non-complex stations are as shown in Figure 2.5. At the end of this classification, 205 stations are classified as complex and 631 stations are non-complex. Complex stations are concentrated in

the Black Sea Region, especially Eastern Black Sea as expected, while non-complex stations are generally concentrated in the Central Anatolian Region.

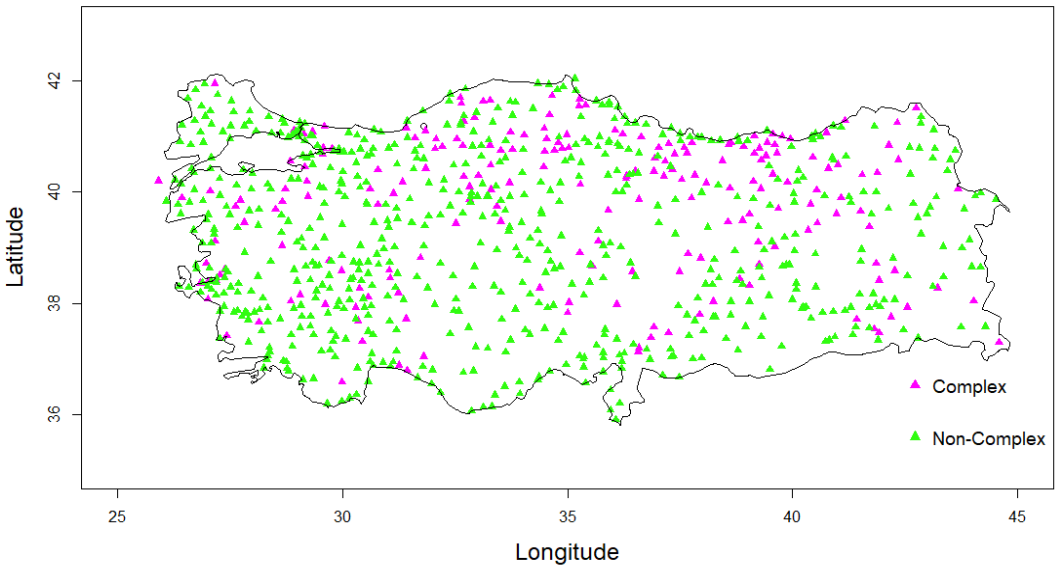

Figure 2.5. Locations of stations by topographical type

2.3.4 Classification of Observed Precipitation Data as Convective and Stratiform

Churchill and Houze (1984) determined precipitation above 20 mm/h as the threshold value for convective precipitation. Similarly, Xu (1995) suggested this value as 10-25 mm/hour, and Dutton and Dougherty (1979) and Watson (1982) suggested this value as approximately 50 mm/hour. The common point of all these values is the possibility that convective precipitation did not rain homogeneously in the same hour. Therefore, a smaller scale is required for analysis.

In the direction of the literature, Llasat (2001) suggests that convective precipitation is greater than 2.92 mm (35 mm/hr) in a 5-minute time interval, which is consistent as the threshold value is in the range of 10-50 mm/hr compared to others. This study (Llasat, 2001) was carried out in Barcelona, Spain and had a mediterranean climate that shows several characteristics in common with Turkey. January is the wettest

month (~96 mm) and July is the driest month (~22 mm) in Barcelona, where the annual average precipitation is approximately 565 mm. (Servei Meteorológic de Catalunya). In this context, in this study, if the precipitation value is greater than 2.92 mm in 5 minutes, it is classified as convective. If it is small, it is classified as stratiform precipitation.

The minutely station data received from TSMS is converted to 5-minutely and the convective-stratiform distinction is made on this dataset. After the seggregation is made, the reference dataset is made ready for analysis by converting it to hourly and daily forms.

2.4 Evaluation Metrics

All products (ALARO, CFS, ECMWF HRES, GFS, WRF) are evaluated and compared separately in daily, monthly and annual time scales. On the hourly time scale, evaluations are made with the available products (CFS, ECMWF HRES, GFS).

2.4.1 Hourly Scale

All five products are evaluated in a daily scale. Precipitation statistics, categorical performance indices, intensity-frequency distributions and seasonal spatial distribution maps are prepared. In addition, all these statistics and distribution maps have been prepared to evaluate the accuracy on a seasonal basis.

The existing 3 model products (CFS, ECMWF HRES and GFS) are evaluated in hourly scale. In order to measure the performance of the hourly datasets of the models, precipitation statistics, categorical performance indices, and intensity-frequency distributions are performed.

2.4.1.1 Precipitation Statistics

The verification of five different precipitation datasets (ALARO, CFS, ECMWF HRES, GFS, WRF) for 3 types of precipitation (total, convective, large-scale) is carried out concerning the station dataset. Daily mean evaluation statistics include mean (Equation 2.1), standard deviation (SD) (Equation 2.2). At the same time, error statistics; bias (Equation 2.3), root mean square error (Equation 2.4), standard deviation of the error (ERRor Standard Deviation, ErrSD) (Equation 2.5) and correlation coefficient (CC) (Equation 2.6) and signal aspect ratio (Signal to Noise Ratio, SNR) (Equation 2.7) is evaluated with the help of the following equations:

$$\mathrm{MEAN_n} = \frac{1}{t}\sum_{i=1}^{t} P_i \qquad 2.1$$

$$\mathrm{SD_n} = \sqrt{\frac{1}{t}\sum_{i=1}^{t}(P_i - \overline{P}_n)} \qquad 2.2$$

$$\mathrm{BIAS_n} = \frac{1}{t}\sum_{i=1}^{t} P_{p,i} - \frac{1}{t}\sum_{i=1}^{t} P_{o,i} \qquad 2.3$$

$$\mathrm{ErrSD_n} = \mathrm{SD}\left[\sum_{i=1}^{t}\left(P_{p,i} - P_{o,i}\right)\right] \qquad 2.4$$

$$\mathrm{RMSE} = \sqrt{\frac{1}{t}\sum_{i=1}^{t}\left(P_{p,i} - P_{o,i}\right)^2} \qquad 2.5$$

$$CC_n = \frac{\sum_{i=1}^{t}(P_{p,i} - \overline{P}_p)(P_{o,i} - \overline{P}_o)}{\sqrt{\sum_{i=1}^{t}(P_{p,i} - \overline{P}_p)^2} \cdot \sqrt{\sum_{i=1}^{t}(P_{o,i} - \overline{P}_o)^2}} \quad 2.6$$

$$SNR_n = \frac{2 * CC}{(SD_x/SD_y + SD_y/SD_x - 2 * CC)} \quad 2.7$$

To the n station numbers in the equations; t day; The "o" and "p" subscripts correspond to the observation and the model, respectively.

$P_{p,i}$ model precipitation prediction (mm/day);

$P_{o,i}$ observed precipitation (mm/day);

$\overline{P}_p$ model mean precipitation (mm/day);

$\overline{P}_o$ observed mean precipitation (mm/day);

SD_x and SD_y are the standard deviations of the observations and models,

respectively.

2.4.1.2 Categorical Performance Indices

Categorical performance indices allow to commenting on the precipitation detection capabilities of the models (Duzenli et al., 2021). Categorical performance indices are calculated to compare the performances of the models for each precipitation type. These are detection probability (Probability of Detection, POD) (Equation 2.8), false alarm rate (False Alarm Ratio, FAR) (Equation 2.9), critical success index (Critical Success Index, CSI) (Equation 2.10) and percent correct (Percent Correct, PC)

(Equation 2.11). These categorical performance indices are calculated as:

$$\mathrm{POD} = \frac{\mathrm{H}}{\mathrm{H} + \mathrm{M}} \tag{2.8}$$

$$\mathrm{FAR} = \frac{\mathrm{F}}{\mathrm{H} + \mathrm{F}} \tag{2.9}$$

$$\mathrm{CSI} = \frac{\mathrm{H}}{(\mathrm{H} + \mathrm{M} + \mathrm{F})} \tag{2.10}$$

$$\mathrm{PC} = \frac{\frac{\mathrm{H}}{\mathrm{CN}}}{\mathrm{E}} \tag{2.11}$$

H is a hit, it is the case of predicting the presence of precipitation correctly in the observation and forecast, and M is a miss. It is the case of the model estimating no precipitation when there is precipitation in the observation. F is a false alarm situation when the model makes predictions in the direction of precipitation when there is no precipitation in the observation and E is the total number of prediction (Table 2.2).

Table 2.2. Algorithm for categorical performance indices

		Observation	
		Above Threshold	Below Threshold
Product	Above Threshold	Hit, H	False alarm, F
	Below Threshold	Miss, M	Correct negative, CN

2.4.2 Daily Scale

All five products are evaluated on a daily time scale. Precipitation accuracy statistics, categorical performance indices, and intensity-frequency distributions are performed to compare the performances. Also, complex and non-complex station classifications are obtained, and the same evaluations are performed (precipitation accuracy statistics, categorical performance indices, and intensity-frequency distributions). Subsequently, these daily datasets are converted to monthly, seasonal, and annual forms. In monthly accumulated data, time series and false alarm ratios are shown for each precipitation type. In seasonal and annual scales, spatial distribution maps are obtained to demonstrate spatial variation. In addition, precipitation statistics are evaluated on a seasonal basis.

CHAPTER 3

RESULTS AND DISCUSSION

The evaluation of precipitation data acquired from five different real-time model data is carried out with the observation data provided by the stations on a daily, hourly, monthly and annual scale. Obtained results are shown and interpreted in the following.

Evaluations of hourly (Observation, CFS, ECMWF HRES, GFS) and daily (Observation, ALARO, CFS, ECMWF HRES, GFS, WRF) available data are discussed below. In addition to mean and standard deviation values, precipitation error statistics, intensity histograms and spatial distribution maps are also included and discussed.

3.1 Hourly Scale

The assessment of the hourly precipitation time series across the country is carried out for 6 years (2015-2020) and the products other than WRF and ALARO are compared. Percentages of precipitation components in available hourly datasets are shown in Figure 3.1. There is a huge difference between station-based observations and model-based product percentages in the convective component of the precipitation. The most striking point is that the percentage of convective precipitation is less than 25 percent in hourly station-based observations.

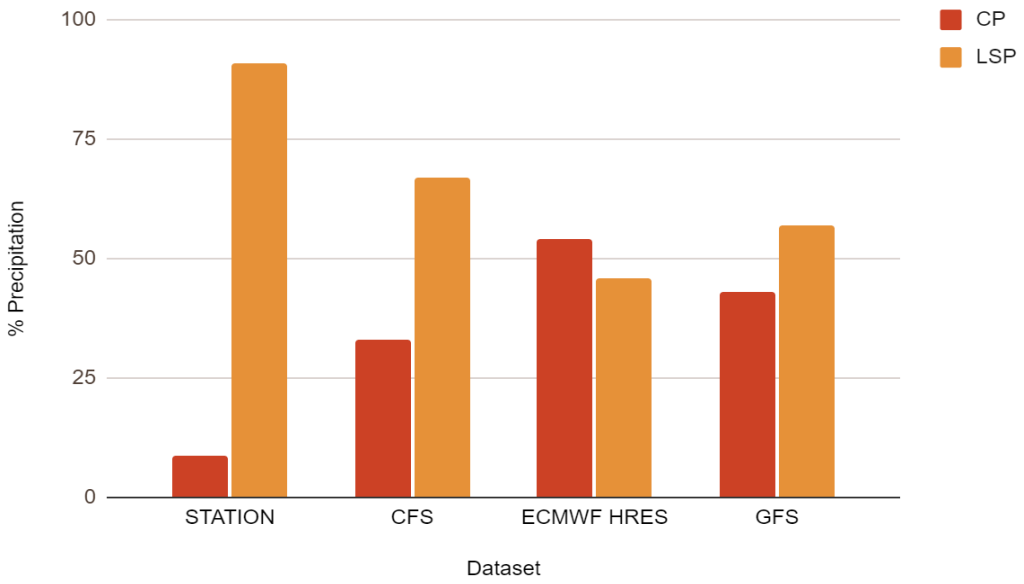

Figure 3.1. Percentages of hourly available datasets

3.1.1 Accuracy Statistics

In the hourly data of total and convective precipitation, ECMWF HRES gave the closest deviation values to the observation (Table 3.1). In large-scale precipitation, the CFS product obtained results closer to the observation in mean and standard deviation (0.06 mm/hr and 0.26 mm/hr, respectively).

When precipitation is divided into convective and large-scale components, it is deduced that the GFS product has the highest ErrSD, RMSE and Bias values (Table 3.2) which may be related to its coarse resolution. Correlations on this time scale are low due to the infrequent precipitation (Table 3.3). At the same time, since convective precipitation is short-term and small-scale heavy precipitation, it is more challenging to get accurate predictions between models at this scale. Moreover, lowest SNR value of large-scale precipitation is observed in ECMWF HRES (0.0963 mm/hr) products since it has the least percentage in Figure 3.1. However, it has the highest SNR values for total and convective precipitations (0.3986 mm/hr and 1.0312 mm/hr, respectively).

Table 3.1. Mean and standard deviation values of hourly datasets

	Dataset	TP	CP	LSP
Mean (mm/hr)	**Observation**	0.0720	0.0057	0.0663
	CFS	0.0910	0.0298	0.0611
	ECMWF	0.0817	0.0415	0.0402
	GFS	0.0799	0.0355	0.0445
Standard Deviation (mm/hr)	**Observation**	0.5534	0.2649	0.4256
	CFS	0.3043	0.1193	0.2575
	ECMWF	0.3320	0.2163	0.2040
	GFS	0.3093	0.1639	0.2473

Table 3.2. Bias, ErrSD and RMSE values of hourly datasets

	Dataset	TP	CP	LSP
Bias (mm/hr)	**CFS**	0.0190	0.0242	-0.0051
	ECMWF	0.0098	0.0359	-0.0261
	GFS	0.0080	0.0299	-0.0218
ErrSD (mm/hr)	**CFS**	0.5535	0.2939	0.4193
	ECMWF	0.5506	0.3458	0.3967
	GFS	0.5440	0.3131	0.4089
RMSE (mm/hr)	**CFS**	0.5514	0.2922	0.4183
	ECMWF	0.5502	0.3437	0.3957
	GFS	0.5427	0.3111	0.4078

Table 3.3. CC and SNR ratios of hourly datasets

	Dataset	TP	CP	LSP
CC with the observation	**CFS**	0.2966	0.0529	0.3348
	ECMWF	0.3119	0.0444	0.3736
	GFS	0.3157	0.0538	0.3566
SNR with the observation	**CFS**	0.3273	0.5282	0.3623
	ECMWF	0.3986	1.0312	0.0963
	GFS	0.3353	0.7658	0.3031

3.1.2 Categorical Performance Indices

When the performance indices for hourly data sets are examined in Figure 3.2, it is observed that the probability of detection (POD) is around 0.4 for all precipitation types. It shows that the models successfully detect precipitation in hourly datasets analysis. However, high false alarm ratio (FAR) values and low critical success index (CSI) values support each other. These results are not unexpected in hourly analyses because the scale is relatively small. Another notable point is there are no apparent outliers in total precipitation CPI. Although the values are close, In convective and stratiform precipitation, the highest POD belongs to the GFS model (Figure 3.2 (d)). It demonstrates the success of GFS in catching hourly precipitation. However, low CSI and high FAR values with a narrow interquartile range in convective precipitation show that model products are not successfully catching the dry hours (Figure 3.2 (e) and Figure 3.2 (f)). Moreover, the CFS product has so many outliers than the others in FAR and CSI values of convective precipitation, it does not normally distributed. The ECMWF HRES has the lowest FAR value in hourly stratiform precipitation, which is successful detecting the dry hours. All model products almost show no outliers in CPI for stratified precipitation. Overall, the data skewnesses are generally normally distributed and less dispersed in all CPI. These results are also underlines, especially in convective precipitation, high FAR and low

POD and CSI values in all types of precipitation can be misleading as there is too much data in this time scale.

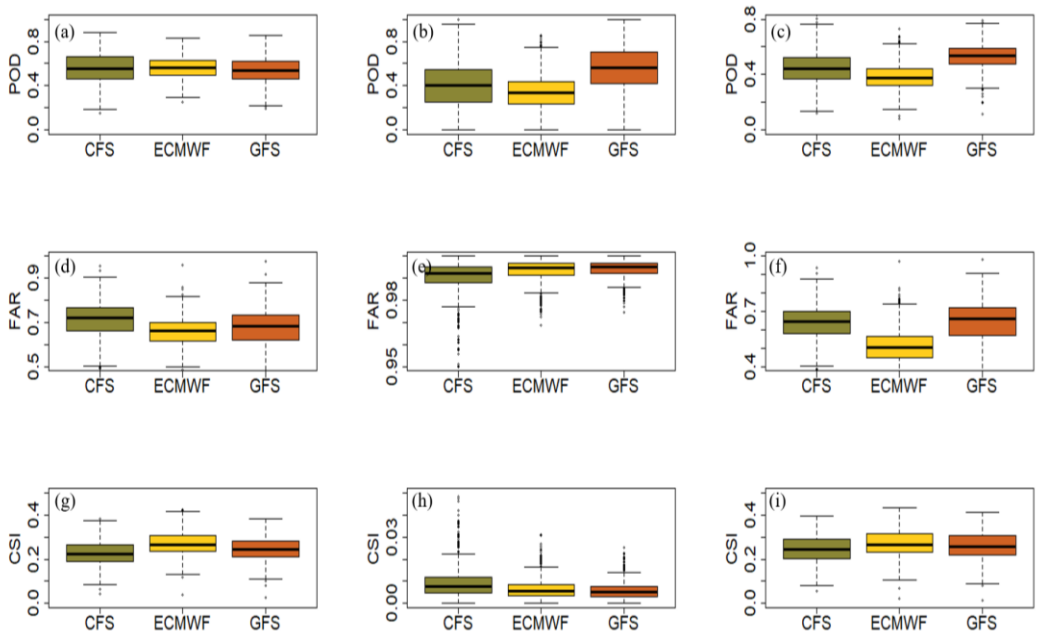

Figure 3.2 POD, FAR, CSI values of hourly precipitation datasets ((a), (d), (g) for total precipitation, (b), (e), (h) for convective precipitation, (c), (f), (i) for stratiform precipitation)

3.1.3 Intensity-Frequency Histograms

Hourly datasets distributions for the years between 2015 and 2020 are shown below. Due to the small hourly scale, similar distributions emerged between station-based observations and model-based products. While total and large-scale distributions primarily pursue the same path (Figure 3.3, Figure 3.5), convective precipitation has a slightly higher distribution in lighter intensities (Figure 3.4). All model products overestimate the convective precipitation, but even so, the CFS product has the closest intensity distribution to the station-based dataset. Model products have a spread close to reference data, as there are so many data in six years on an hourly scale. Overall, the CFS product has the highest accuracy while matching these light intensity frequencies, while the GFS product has a more linear distribution than

observation for the convective precipitation. In the large-scale precipitation distributions, it can be seen that GFS product underestimated, ECMWF HRES slightly overestimated in lighter intervals.

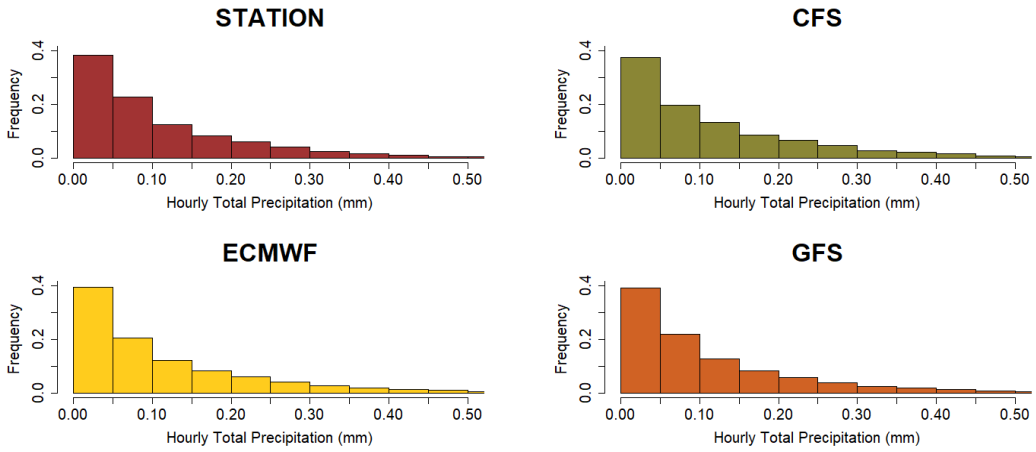

Figure 3.3. Hourly total precipitation histograms for 2015-2020

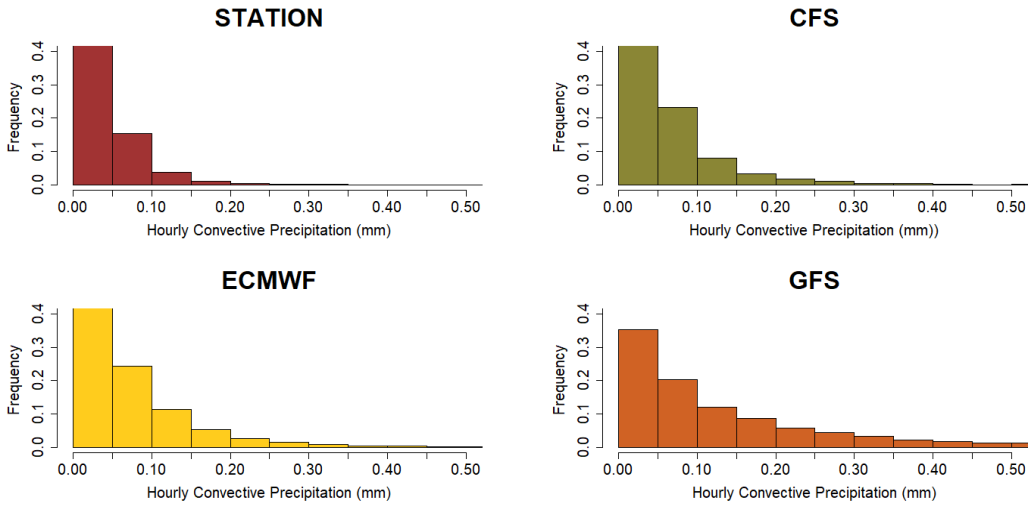

Figure 3.4. Hourly convective precipitation histograms for 2015-2020

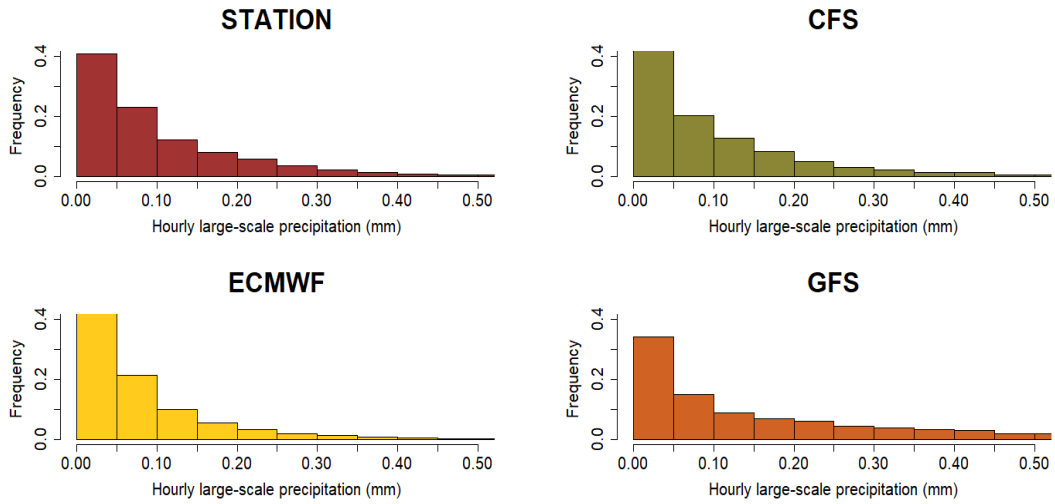

Figure 3.5. Hourly large-scale precipitation histograms for 2015-2020

3.2 Daily Scale

The daily precipitation time series assessment across the country is carried out for 4 years (2015-2018) with all available products (ALARO, CFS, ECMWF HRES, GFS and WRF). Figure 3.6 illustrates the percentages of convective and stratiform precipitations in available daily datasets. As on the hourly scale, ECMWF HRES shows the highest convective precipitation percentage higher than other model producs. Ratios are close to each other among other model-based datasets. Moreover, station-based observation dataset has a remarklable percentage difference same with the hourly scale.

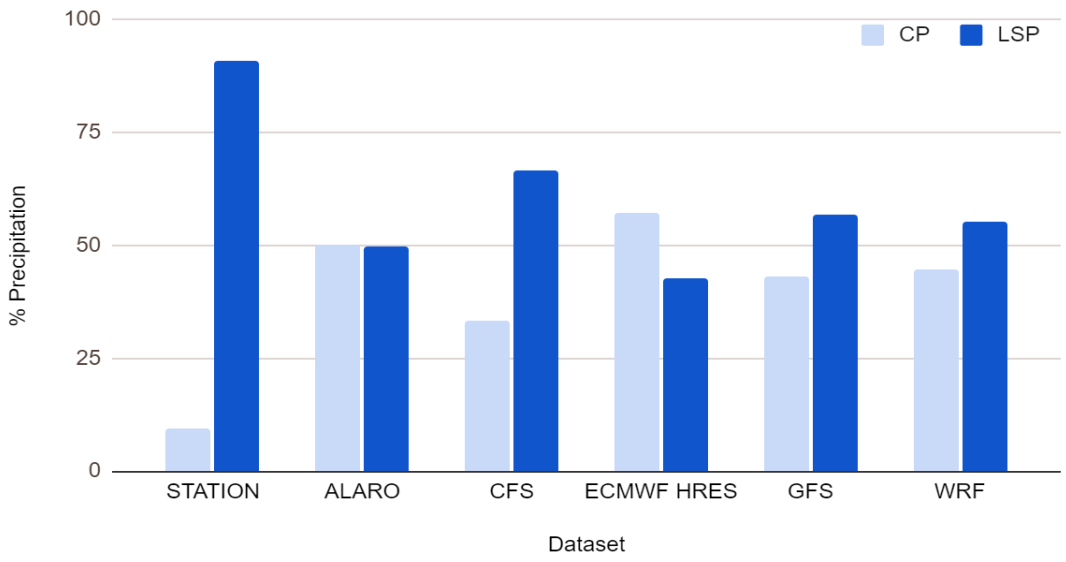

Figure 3.6. Percentages of precipitation components in daily datasets

3.2.1 Accuracy Statistics

The products in the daily precipitation datasets showed relative mean and standard deviation values in total precipitation and its stratiform component (Table 3.4). For total and convective precipitation GFS and ALARO, for stratiform precipitation CFS product has the lowest bias values (Table 3.5). While the CFS product has the lowest ErrSD and RMSE values for the convective component of the precipitation, ECMWF HRES has the lowest ErrSD and RMSE values for total and stratiform precipitations (Table 3.5). Furthermore, ECMWF HRES has the highest correlation (CC) for total and large-scale precipitation (0.67 and 0.65, respectively), WRF has the highest CC for convective precipitation (0.21) in Table 3.6. The CC values for convective precipitation are low since it is very tough to catch for NWP models and meteorological stations; this kind of precipitation has a high intensity but in a small area and duration. High SNR values of convective precipitation also support these results which are below 0.25

Table 3.4. Mean and standard deviation values of daily datasets

	Dataset	TP	CP	LSP
Mean (mm/day)	**Observation**	1.79	0.16	1.64
	ALARO	1.60	0.74	0.96
	CFS	2.29	0.79	1.50
	ECMWF	2.02	1.07	0.95
	GFS	1.94	0.90	1.04
	WRF	2.10	0.90	1.20
Standard Deviation (mm/day)	**Observation**	5.66	1.79	4.79
	ALARO	4.79	2.61	2.92
	CFS	5.35	2.21	4.37
	ECMWF	4.68	2.57	2.96
	GFS	4.72	2.58	3.62
	WRF	5.55	3.06	4.03

Table 3.5. Bias, ErrSD and RMSE values for daily datasets

	Dataset	TP	CP	LSP
Bias (mm/day)	**ALARO**	-0.20	0.59	-0.68
	CFS	0.50	0.63	-0.14
	ECMWF	0.23	0.92	-0.69
	GFS	0.14	0.75	-0.60
	WRF	0.31	0.75	-0.44
ErrSD (mm/day)	**ALARO**	4.99	3.13	3.73
	CFS	5.17	2.83	4.12
	ECMWF	4.41	3.05	3.62
	GFS	4.91	3.11	3.92
	WRF	5.00	3.41	3.86
RMSE (mm/day)	**ALARO**	5.02	3.20	3.80
	CFS	5.28	2.92	4.18
	ECMWF	4.44	3.21	3.69
	GFS	5.00	3.22	4.00
	WRF	5.03	3.51	3.90

Table 3.6. CC and SNR ratios for daily datasets

	Dataset	TP	CP	LSP
CC with the observation	**ALARO**	0.58	0.15	0.63
	CFS	0.60	0.19	0.61
	ECMWF	0.67	0.17	0.65
	GFS	0.61	0.17	0.61
	WRF	0.63	0.21	0.63
SNR with the observation	**ALARO**	1.52	0.15	1.41
	CFS	1.53	0.20	1.61
	ECMWF	2.09	0.17	1.50
	GFS	1.48	0.17	1.42
	WRF	1.79	0.20	1.76

Table 3.7 show the cross-correlation values of available NWP model datasets. Results reveal the similarity between the model datasets. It is seen that convective precipitation has lower correlation values than the other two precipitations. This can be attributed to the fact that each model has convective precipitation parameters with different sensitivity. When all correlation values are examined, it is seen that the highest values are between ECMWF HRES and WRF model products in all

Table 3.7. Cross-correlation values of the NWP models

	CC		
Datasets	**TP**	**CP**	**LSP**
ALARO-CFS	0.60	0.42	0.59
ALARO-ECMWF	0.68	0.54	0.63
ALARO-GFS	0.58	0.40	0.58
ALARO-WRF	0.62	0.46	0.60
CFS-ECMWF	0.75	0.57	0.73
CFS-GFS	0.75	0.59	0.77
CFS-WRF	0.66	0.56	0.66
ECMWF-GFS	0.75	0.56	0.77
ECMWF-WRF	0.79	0.61	0.78
GFS-WRF	0.66	0.53	0.68

3.2.2 Categorical Performance Indices

In the study area, the distributions of daily categorical performance indices for all three precipitation types are given in the figures below. For the daily total precipitation, all model products gave a high percentage of correct values (PC>0.7) (Figure 3.7). At the same time, values close to 1 are presented by all products, especially ECMWF HRES for POD and CSI. This indicates the success of the model products in predicting wet days. The models have almost the same values for the FAR, but it is clear that ALARO has a value closest to 0 (FAR<0.4). In this case, ALARO is more successful than other products in predicting dry days in daily total precipitation. Model products show significant outliers in total precipitation since these datasets have the largest sample size. In addition to the high FAR values for convective precipitation, the CSI values of all products are also supportively low (Figure 3.8). These results indicate that the PC values of the ALARO and WRF models are relatively high (PC>0.8) compared to the other model products. Among the detection possibilities, the ECMWF HRES has a higher distribution (POD>0.8) than the others, which reveals that the ECMWF product is more successful than other products in predicting wet days in the daily values of convective precipitation. Besides, all model products have an unbalanced lower and upper quartile distance, called whiskers; they also show different thicknesses, meaning they have different spreads of data. Finally, it can be seen in Figure 3.9 that daily large-scale precipitation results in similar values to total precipitation. The highest POD and CSI values of ALARO and ECMWF products can be interpreted as these two models are good at predicting the existence of stratiform precipitation. Likewise, all products except CFS, have low FAR values (FAR<0.4), which means model products are good at predicting dry days. At the same time, the detection probabilities of all models are almost above 0.8, so the products have high POD values, just like the total daily precipitation.

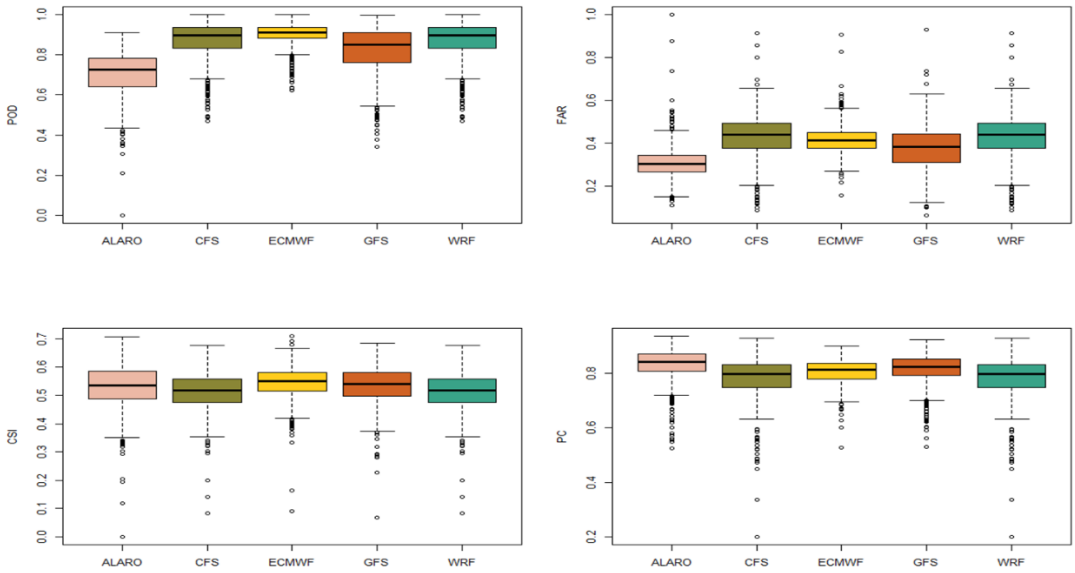

Figure 3.7. CPI for total precipitation of daily data

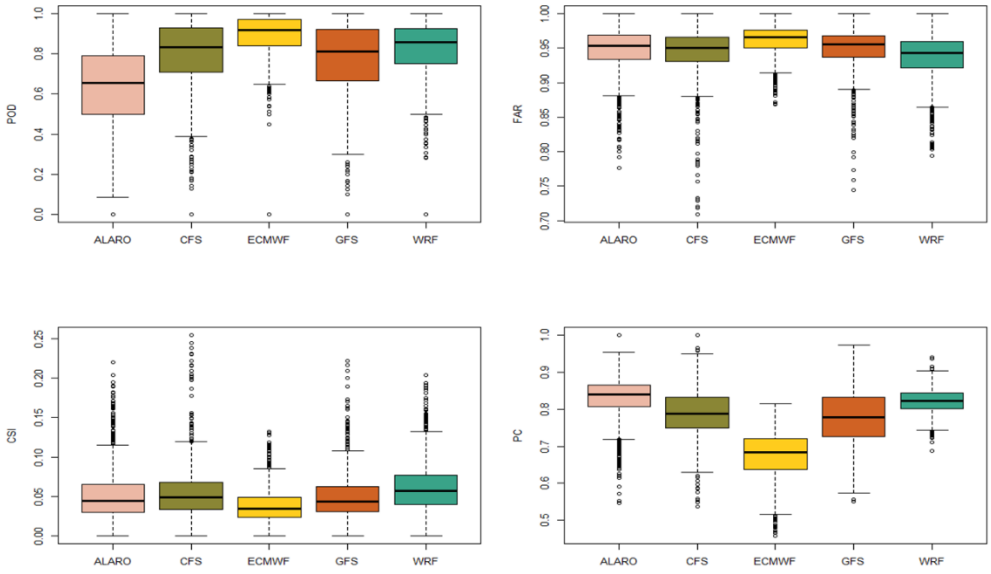

Figure 3.8. CPI for convective precipitation of daily data

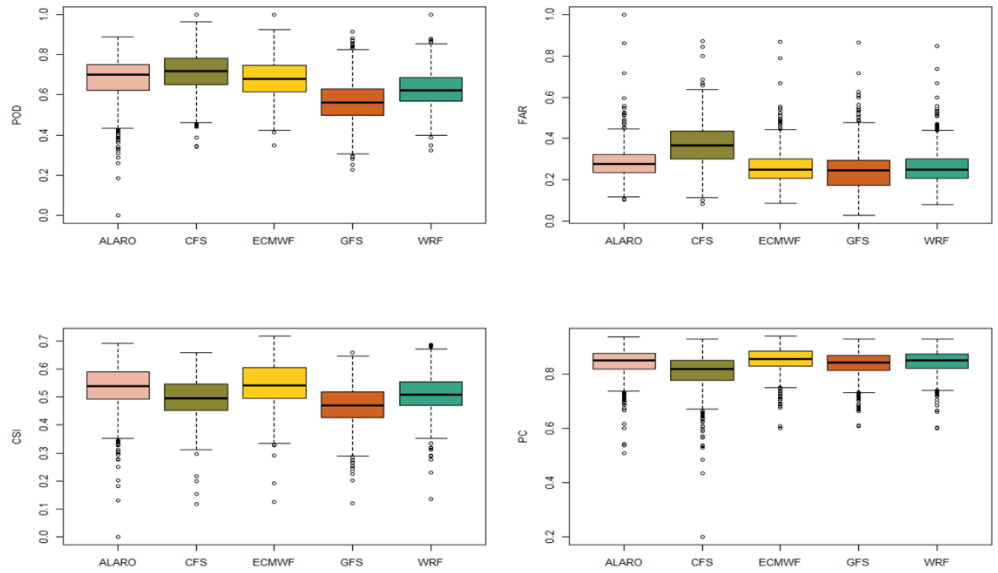

Figure 3.9. CPI for stratiform precipitation of daily data

3.2.3 Intensity-Frequency Histograms

The distributions of the reference data and model products for the 3 precipitation types are as follows. There is a very close distribution between the histograms of the total precipitation years between 2015 and 2018 in Figure 3.10. Moreover, most of the total precipitation is in lighter densities (0-1 mm excluded), and all histograms are right-skewed. CFS product depicts a slight underestimation in total precipitation distribution

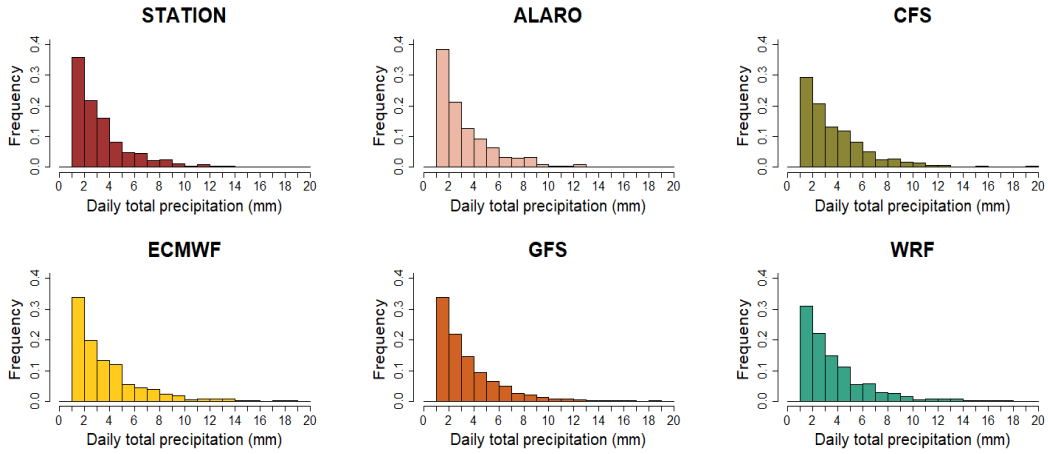

Figure 3.10. Daily precipitation histograms for total precipitation

In the observed distribution of convective precipitation, it is seen that precipitation is collected in the first interval (1-2 mm), excluding the 0-1 mm interval. There is a similar result in model precipitation products, precipitation is at high frequency with light intensities, but they still have a linear distribution. For this reason, although the models showed a different result from the observation, they demonstrated a consistent result among themselves (Figure 3.11).

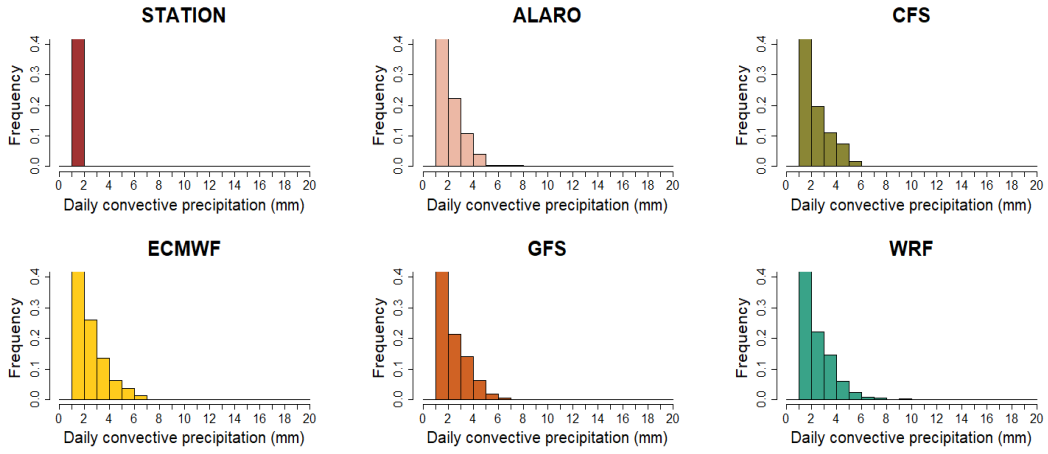

Figure 3.11. Daily precipitation histograms for convective precipitation

Furthermore, there is a consistent linear distribution similar to total precipitation distributions for stratiform precipitation in Figure 3.12. When examined in detail, it is seen that the CFS and WRF models show a closer distribution to the observation than other models. ALARO, GFS and ECMWF HRES have a higher frequency than observation in lighter precipitations.

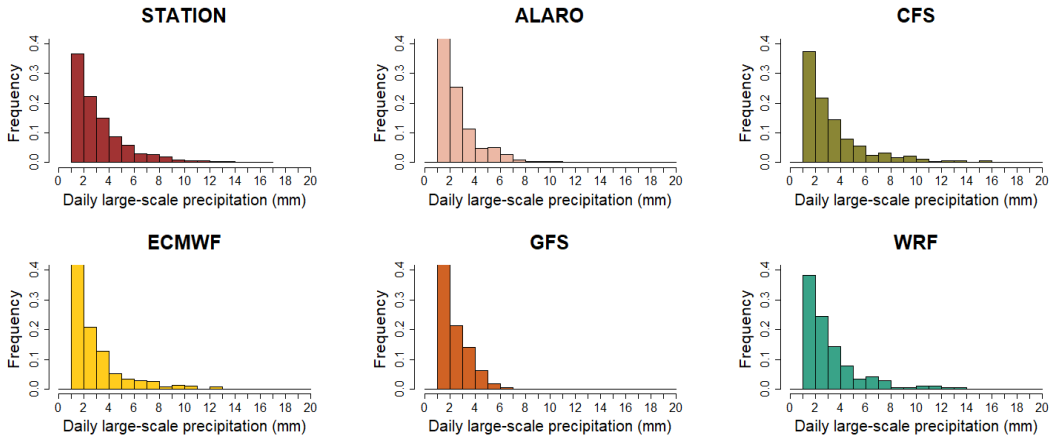

Figure 3.12. Daily precipitation histograms for large-scale precipitation

3.2.4 Evaluation of Complex and non-Complex Regions

3.2.4.1 Accuracy Statistics

The Taylor diagram summarizes three frequently used metrics to evaluate hydrological or climate data (Zhou et al., 2021). These metrics are correlation, root mean square difference, and standard deviation of models and observations (Taylor, 2001). The correlation coefficients are shown with the azimuth angle, and standard deviation with the distance from the origin. Root-mean-square error is centered by subtracting the respective means proportional to the observation point located on the x-axis (Kim and Park, 2016). Thus, bias is not measured in the Taylor diagram. Figure 3.13 covers the Taylor diagrams of the daily total, convective and large-scale precipitations of complex and non-complex areas. Each point indicates the existing

datasets (Observed, ALARO, CFS, ECMWF, GFS and WRF). The correlation values of models are around 0.6 and root-mean-square errors are very similar for both areas of daily total and large-scale precipitations. The closest point to the observation dot is the optimal result corresponding to the most satisfactory performance in the Taylor diagrams. These points show more consistency in total and large-scale precipitations. There is a specific scattering in the models for convective precipitation in complex areas. The distances between the reference point and individual model datasets are much larger when the area is complex. The spread between the azimuth angle and radial direction among the regions indicates the spread in spatial pattern and magnitude. Although the model ECMWF HRES product seems to be the closest to the optimal point, the variation of the correlations between 0.1 and 0.2 reveals that the models are weak in estimating this type of precipitation compared to other precipitations.

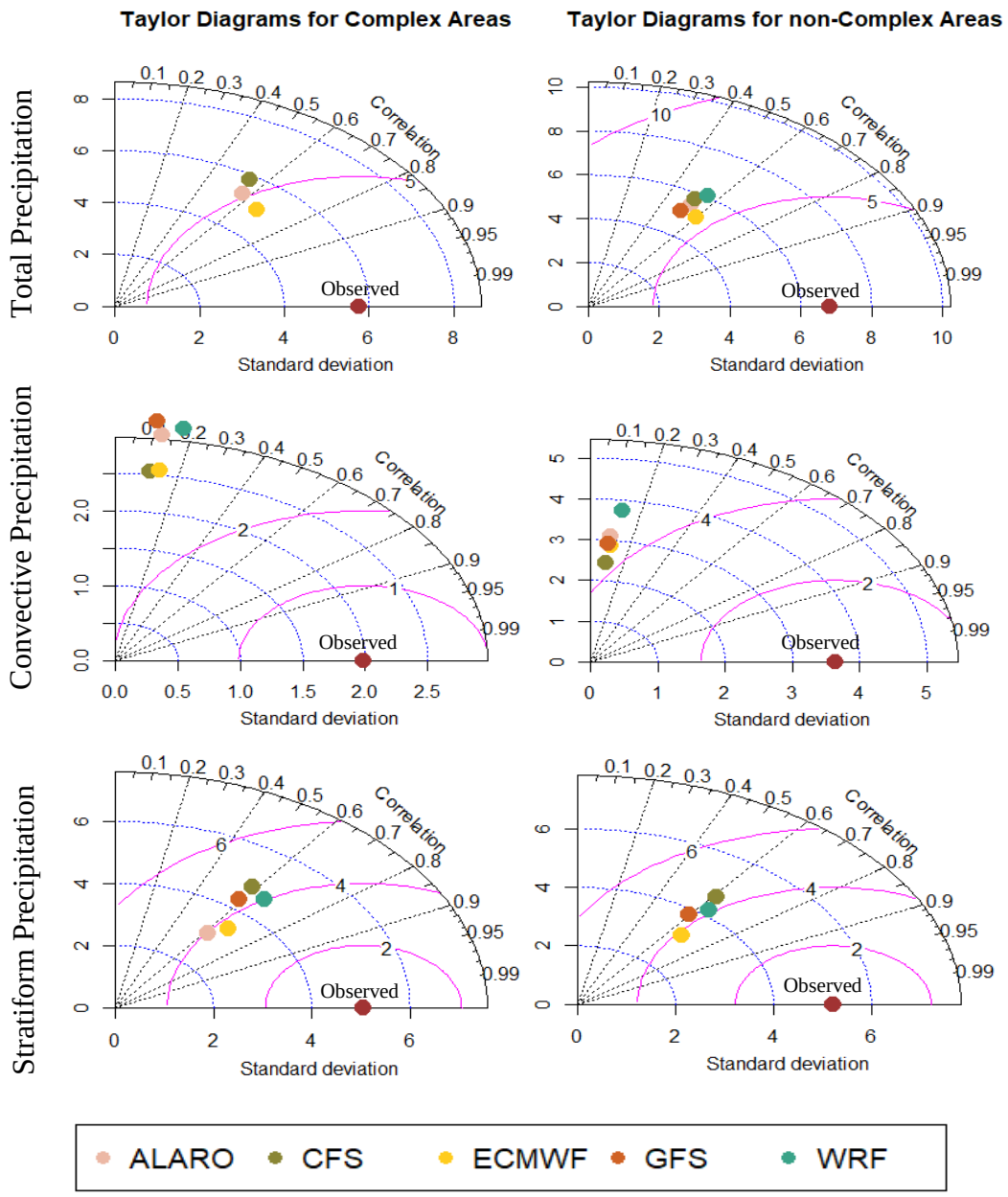

Figure 3.13. Taylor diagram for complex and non-complex areas. Outermost quarter black circle corresponds to correlation coefficients, blue circles to standard deviation values, magenta to root-mean-square error values.

3.2.4.2 Intensity-Frequency Analysis

It is seen in Figure 3.14 and Figure 3.16 that the model products have a similar distribution with the observation in total and stratiform precipitation without dry days (0-1 mm interval) in complex areas, which comprise 205 stations. Although model products have this close trend, the CFS product underestimated total precipitation in lighter intensities. In contrast, convective precipitation in complex areas accumulated at lower intervals in both observation and model products, a considerable amount of the precipitation accumulated in 0-1 mm intervals in observation and all model products are overestimated (Figure 3.15). However, the model products make a consistent estimation of each other. The topography has a significant influence on this result since it has a direct effect on both the reference dataset and model performances. It is also tough to catch short-term and small-area cover convective precipitation by ground observation stations which are in a point form and sparse in complex areas. This situation is observed mainly in the Eastern Black Sea region, where complex stations are concentrated. Since most of the total precipitation belongs to stratiform precipitation, their observed station distribution is also imitative (Figure 3.16). They both show right-skewed distributed histograms. ALARO and ECMWF HRES products again overestimated in lighter intensities (1-2 mm). WRF is the most successful product by capturing low-frequency precipitation at high-intensities close to station observation where the slope is greater than 5%.

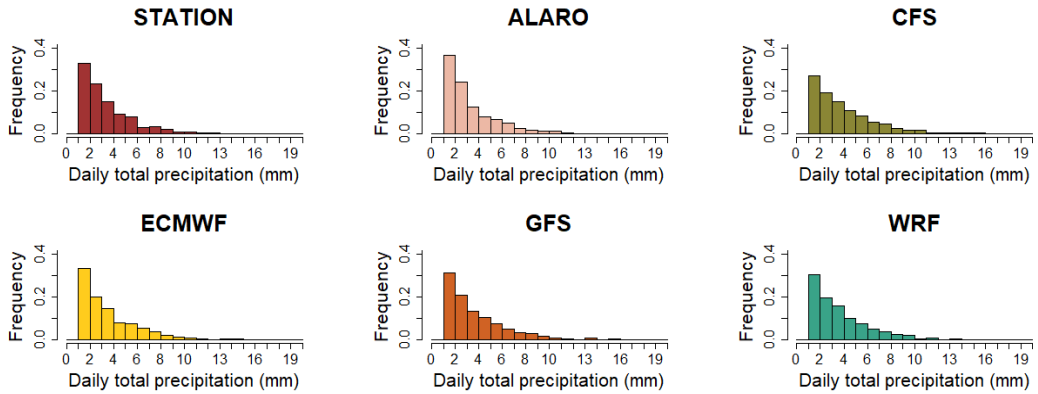

Figure 3.14. Daily precipitation histograms for total precipitation in complex areas

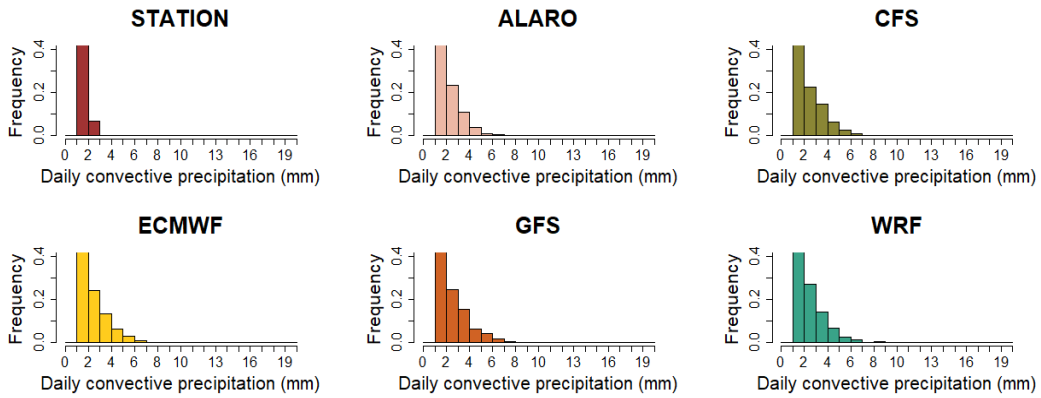

Figure 3.15. Daily precipitation histograms for convective precipitation in complex areas

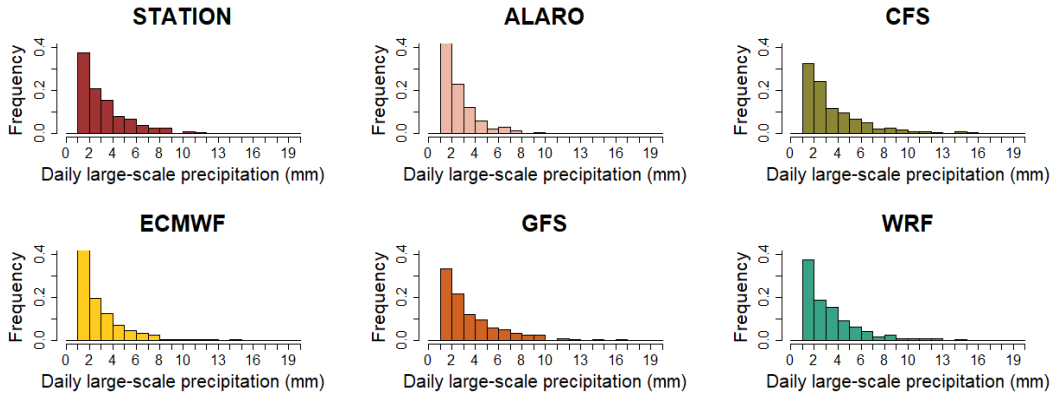

Figure 3.16. Daily precipitation histograms for large-scale precipitation in complex areas

Furthermore, the distribution of total precipitation in 631 non-complex stations is successfully catched by the model products. However, it is observed that the CFS and WRF products underestimate lighter intensities in total precipitation (Figure 3.17). In the convective component of the precipitation, the same result is observed in the non-complex regions; the precipitation in the observation accumulated at low densities for all datasets. Otherwise, products have followed a right-skewed distribution and consistent among themselves (Figure 3.18). Since most of the total precipitation is stratiform, they demonstrated a similar distribution in non-complex areas as well. All models illustrated a successful performance, except for the

overestimation in ALARO and ECMWF HRES products distribution in the 1-2 mm range (Figure 3.19).

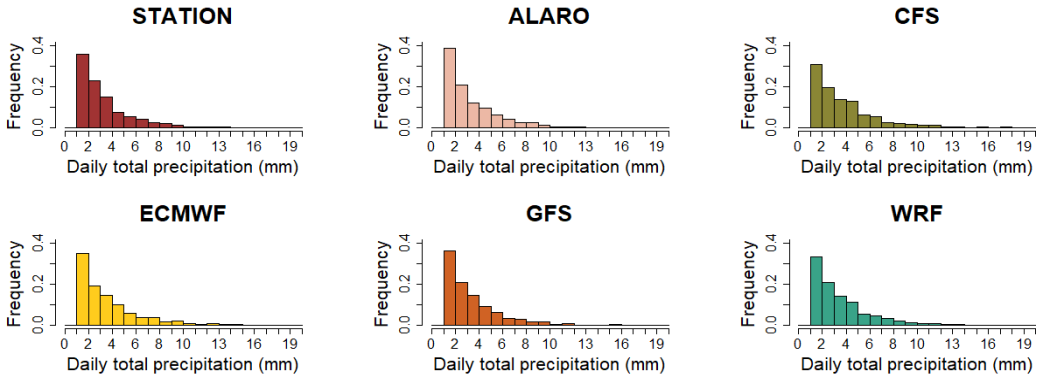

Figure 3.17. Daily precipitation histograms for total precipitation in non-complex areas

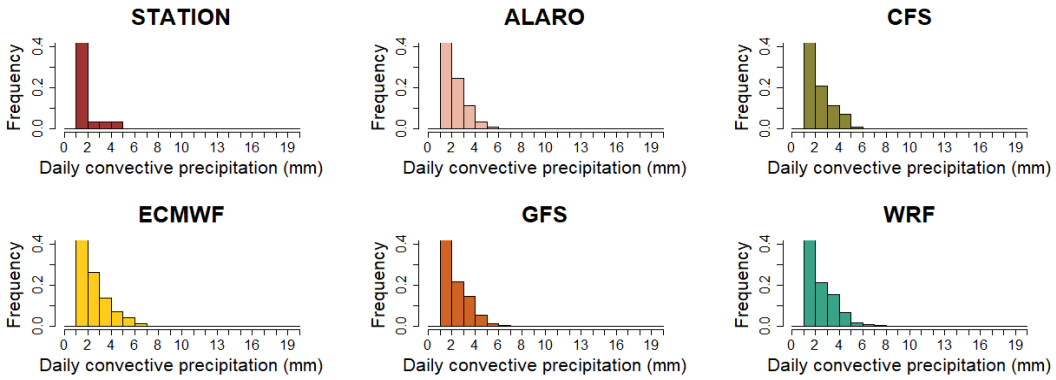

Figure 3.18. Daily precipitation histograms for convective precipitation in non-complex areas

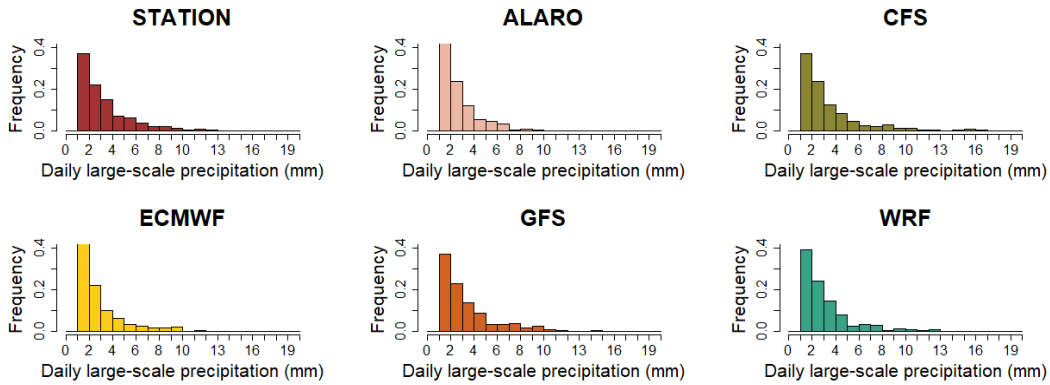

Figure 3.19. Daily precipitation histograms for large-scale precipitation in non-complex areas

3.2.4.3 Categorical Performance Indices

When the categorical performance indices of the models in complex areas are examined, the lower POD and FAR values of the ALARO product for total precipitation stand out (Figure 3.20). Meanwhile, it has the highest PC values, which leads that the ALARO product may be practical for dry day estimations. In convective precipitation distributions (Figure 3.21), model products have almost similar outcomes and the most striking point is the high FAR and low CSI values. However, ECMWF HRES has higher POD and FAR and lower CSI and PC values. From this result, it can be deduced that the ECMWF HRES product overestimates convective precipitation forecasts in complex areas. Hence, it is convenient for wet-day estimation studies.

On the contrary, such high FAR values can adversely affect many operations, especially in an economical way. Subsequently, when the categorical performance indices for stratiform precipitation are examined in 205 stations (Figure 3.22), it is apparent that they have consequent results with total precipitation. As a result, it is revealed that the models performed poorer in capturing high-intensity rapid precipitation than lighter precipitation intensities. This is relatable with a more considerable amount of total precipitation consisting of stratified precipitation.

Overall, the unpredictability of convective precipitation with that much FAR value can cause errors in the measures to be taken in water resource management.

The fact that the ECMWF HRES product has the highest POD (>0.8) value in total precipitation shows that it is successful in wet day forecasts as in complex areas (Figure 3.20). The ALARO product with the lowest FAR value (<0.4) shows a good result in the dry day forecast of total precipitation. Overall, all model products performed well in total precipitation, as expected. In convective precipitation (Figure 3.21), the high FAR values of the models are again one of the most remarkable results. Although the models with high POD values showed good performance in wet day forecasts, they still showed poor results in catching dry days compared to other precipitation components. The ALARO product, which has the highest PC values (>0.7), is partially more successful in flat areas than other models. In the large-scale component of precipitation (Figure 3.22), a result parallel to the total precipitation is evident. The CFS product is more successful in capturing large-scale precipitation as expected, with higher POD values, but the low FAR (<0.3) and high CSI (>0.5) as well as the highest PC (>0.8) result with the highest median value belongs to the ECMWF HRES product.

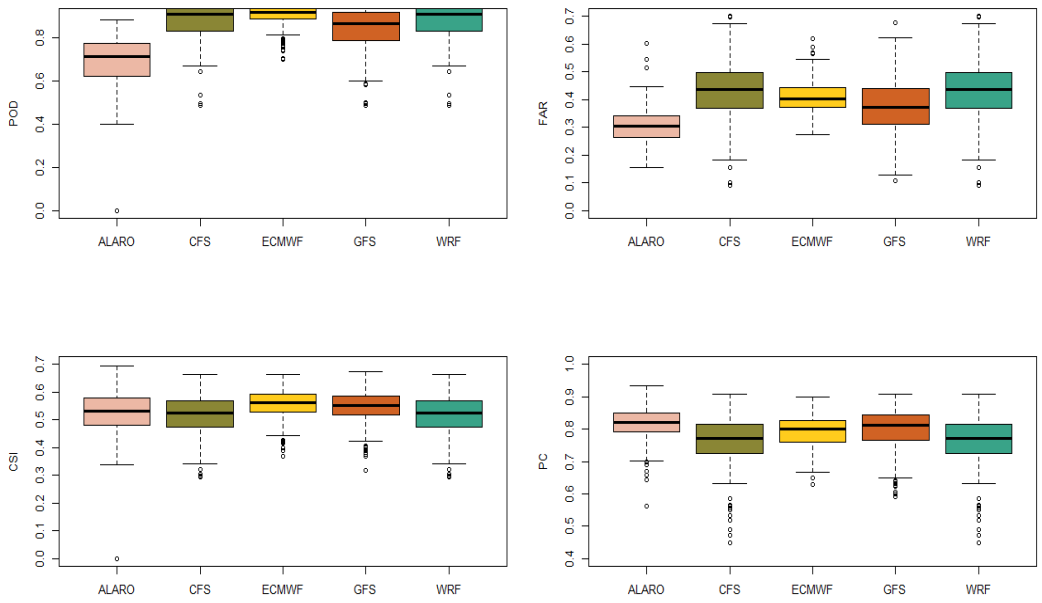

Figure 3.20. CPI for daily total precipitation in complex areas

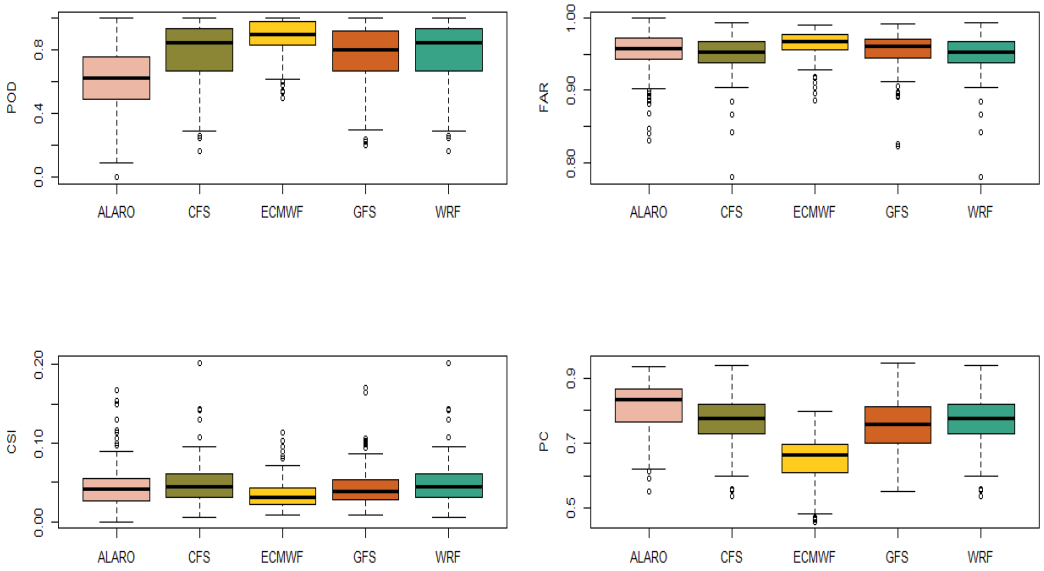

Figure 3.21. CPI for daily convective precipitation in complex areas

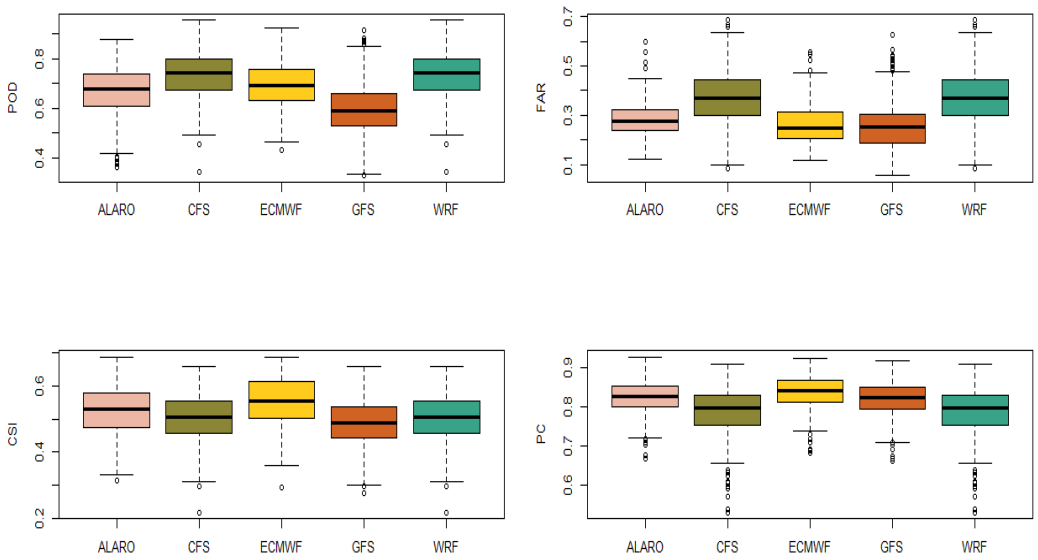

Figure 3.22. CPI for daily large-scale precipitation in complex areas

In non-complex 631 stations (Figure 3.23), for total precipitation, ECMWF HRES shows an obvious highest result in POD, which is higher than 0.8 and ALARO product gives the lowest FAR among others less than 0.4. After investigating the CSI and PC, it can be concluded that all models show a satisfying performance where the topography is flatter. Furthermore, for the convective precipitation CPIs (Figure 3.24), the first noticeable point is models have lots of outliers in FAR and CSI with very high FAR and low CSI results. These results are consistent with other regions. However, ALARO shows slightly lower FAR and higher PC values among the other products. It also has the narrowest interquartile range in all CPIs. In large-scale box plots (Figure 3.25), all models are good performers since they have very high PC and minimal interquartile ranges. Supportively, they have high POD and CSI, and low FAR values. Although they have small interquartile ranges, they have a lot of outliers in each CPI. ALARO and ECMWF HRES are the best two performers with their higher POD, CSI and PC, lower FAR and less outliers.

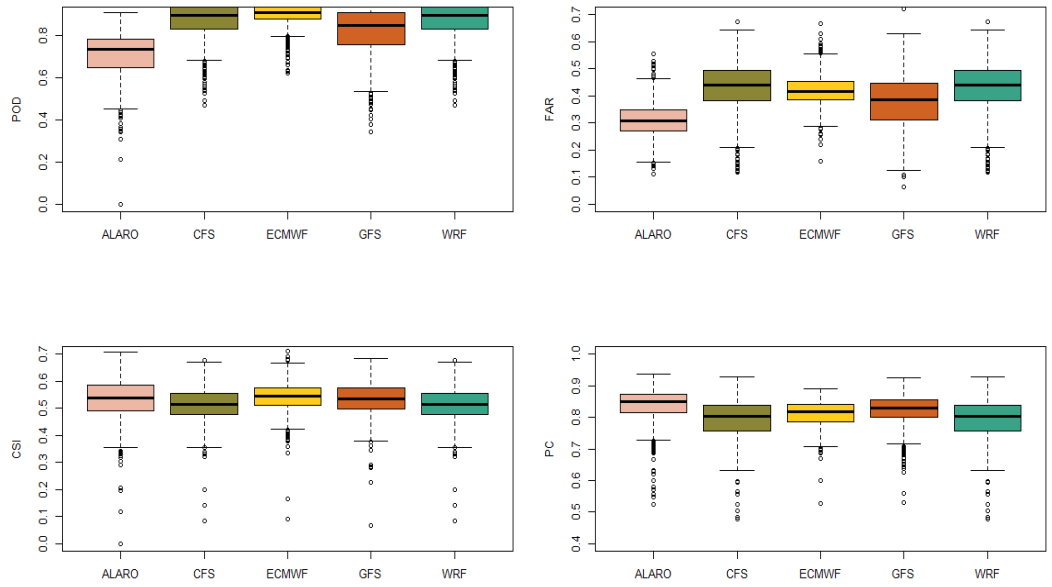

Figure 3.23. CPI for daily total precipitation in non-complex areas

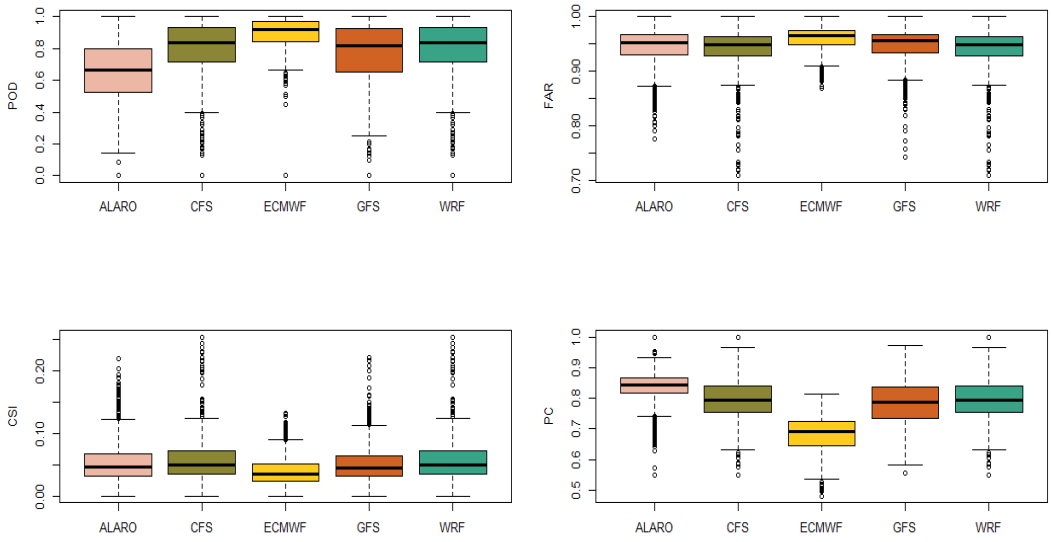

Figure 3.24. CPI for daily convective precipitation in non-complex areas

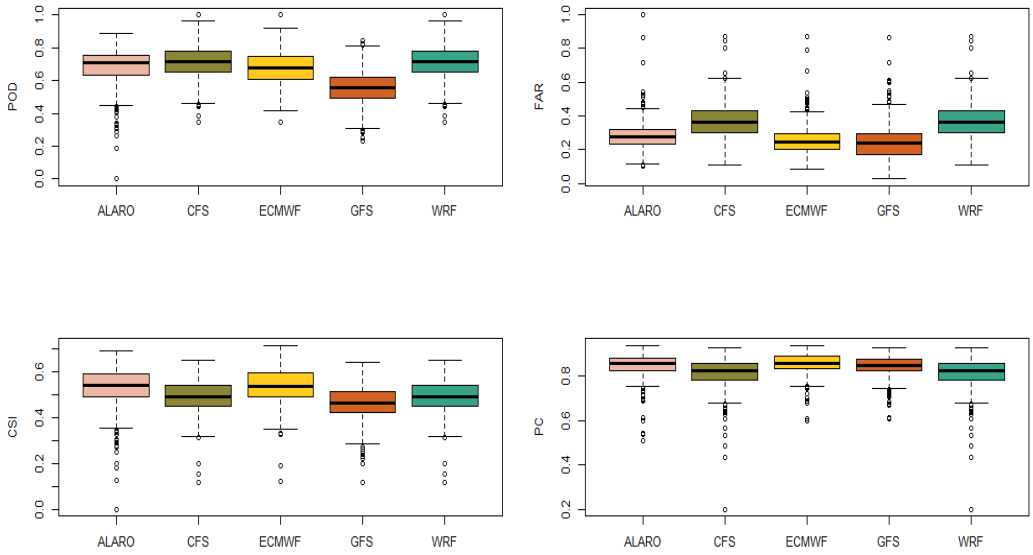

Figure 3.25. CPI for daily large-scale precipitation in non-complex areas

3.2.5 Monthly Scale

Figures 3.26 and 3.27 illustrate monthly total precipitation in complex and non-complex area time series. All model products catch a sharp rise in August 2016 except ALARO in both regions. Although models and station measurements followed the same trends, more precipitation is seen in complex areas. In the summer months of 2017, it was seen that the amount of precipitation was below average. Moreover, in January 2017, the precipitation amount was almost zero, which is catched by all model products. It is also observed that model products other than the ALARO and ECMWF HRES products cause a high amount of overestimation, while the ALARO product occasionally underestimates in both topographies. CFS product makes the most overestimation in both topographies depending on its coarser resolution.

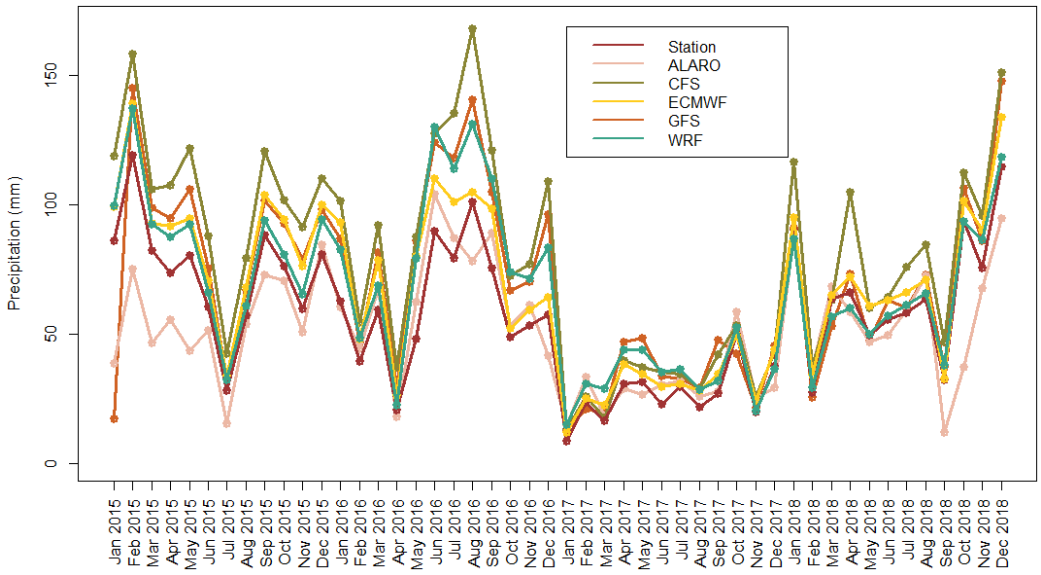

Figure 3.26. Monthly total precipitation for observation and 5 NWP models over complex areas

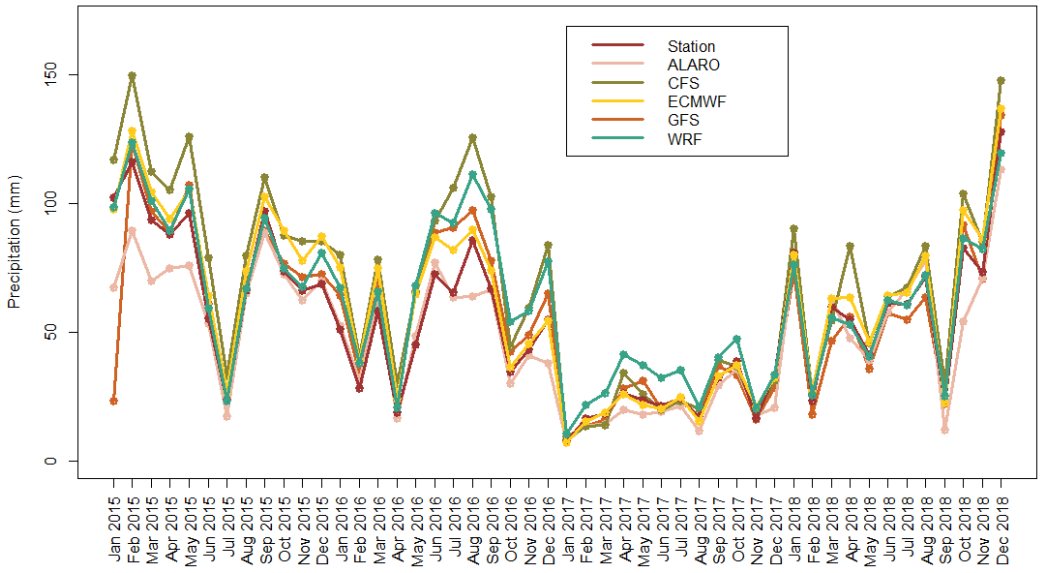

Figure 3.27. Monthly total precipitation for observation and 5 NWP models over non-complex areas

Variability at monthly precipitation time series is investigated in more detail by plotting the convective precipitation for observation and all products (Figure 3.28 and Figure 3.29) for complex and non-complex areas. While the results reveal a significant increase in convective precipitation in both topography types in the summer of 2016, the ALARO product gives the closest result to the observation at this peak point. However, the other model products are consistent among themselves. ECMWF HRES product showed a different behavior from other products in the winter months of 2016, predicting significantly higher precipitation than the observation in both areas. It is expected that convective precipitation will increase in the summer months due to the increase in convection as the weather warms up. Overall, models overestimated the convective precipitation but showed trends similar to the station-based results as the previous results.

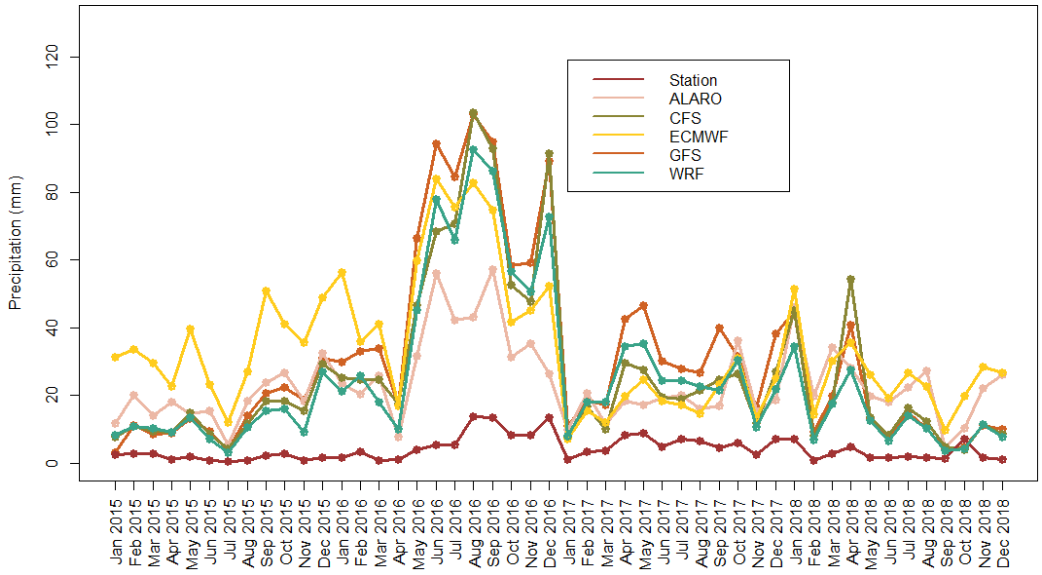

Figure 3.28. Monthly convective precipitation for observation and 5 NWP models over complex areas

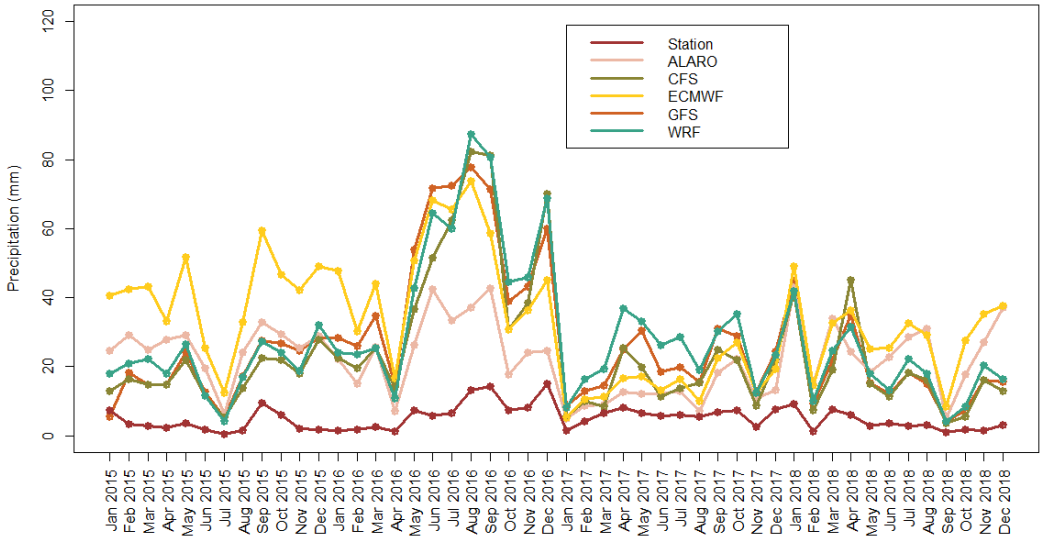

Figure 3.29. Monthly convective precipitation for observation and 5 NWP models over non-complex areas

When Figures 3.30 and 3.31 are examined, it is observed that the distribution of the stratiform component of the precipitation is slightly different from the other two precipitations. First, although the model products followed a similar trend to total precipitation in convective precipitation, stratiform precipitation has slumped in August 2016 until January 2018 in both regions. In addition, it reveals that the trend of station-based observation precipitation is quite similar to that of the total precipitation and larger part of the total precipitation consists of stratified precipitation. Although the model products are close to catching the observation, it is shown that they underestimate the stratiform precipitation for 4 years, especially in 2016 and 2017. However, the product that managed to catch the closest trend is CFS in both complex and non-complex areas.

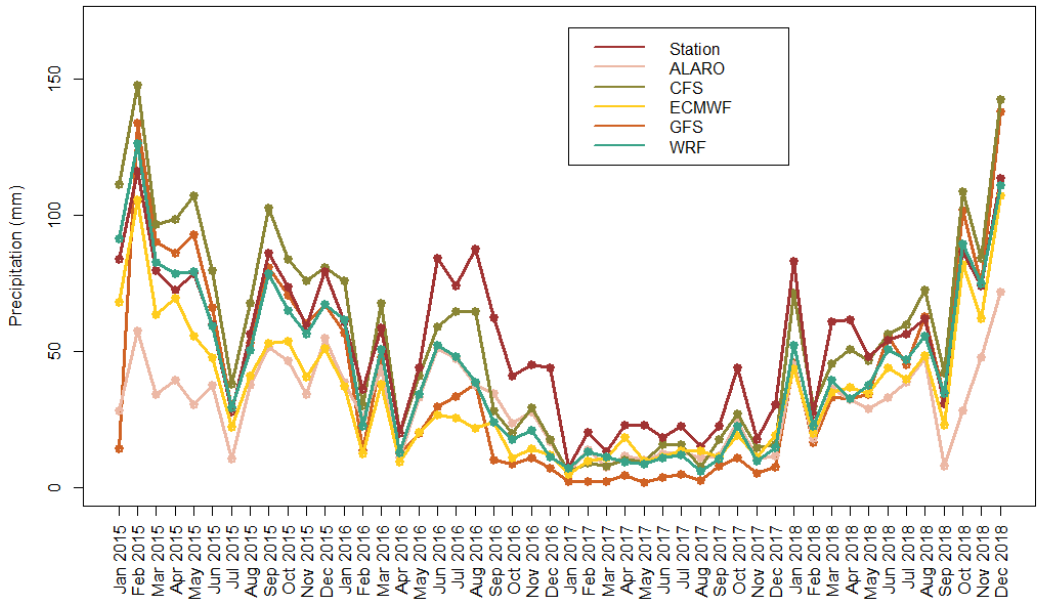

Figure 3.30. Monthly large-scale precipitation for observation and 5 NWP models over complex areas

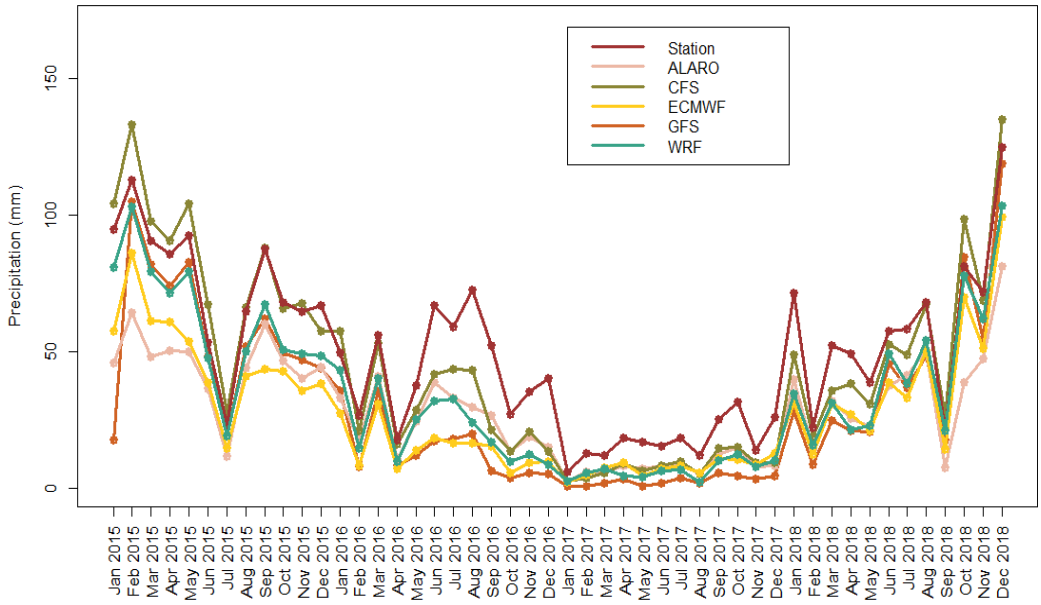

Figure 3.31. Monthly large-scale precipitation for observation and 5 NWP models over non-complex areas

Figure 3.32 illustrates that the monthly average FAR values of the model products in total precipitation follow a similar trend each other. The product with the lowest FAR value is ALARO, which shows its success in catching rainless days. There is a gradual increase between the January and July FAR values. After that, it rapidly decreased until December. The conclusion drawn from this figure is; the models have difficulty catching the times when there is no precipitation compared to the winter months, as convective precipitation prevails throughout our country in summer.

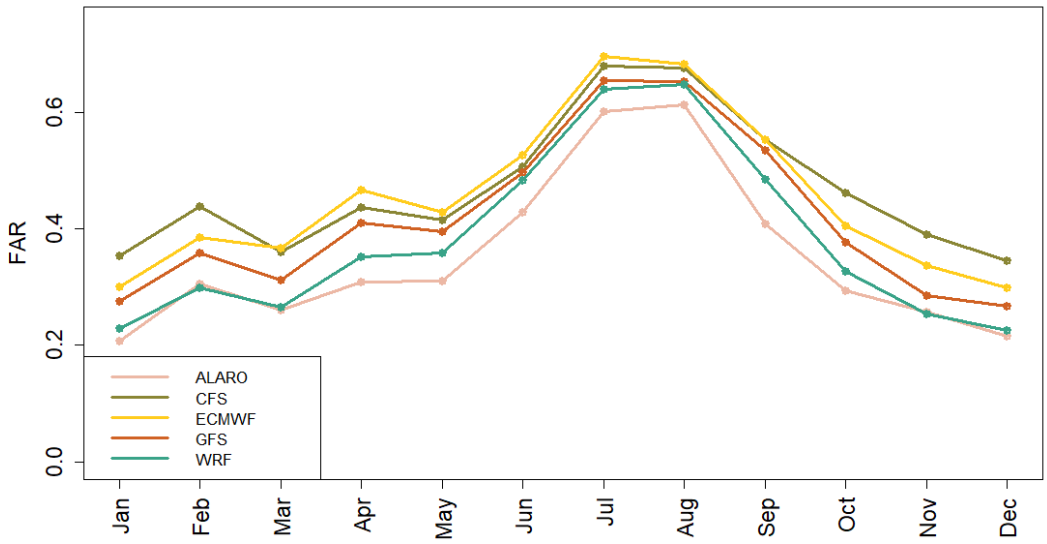

Figure 3.32. Monthly average FAR values of total precipitation in the entire area

Due to the overestimation of convective precipitation in the models, the monthly average of the 4-year FAR values are shown in the Figure 3.33. The FAR values obtained are pretty high; however, due to the dominance of convective precipitation throughout our country in the summer months, it has dramatically declined in the summer months, as expected. The fact that the models catch the trend in FAR but

with high values can be associated with the low amount of precipitation in the reference dataset.

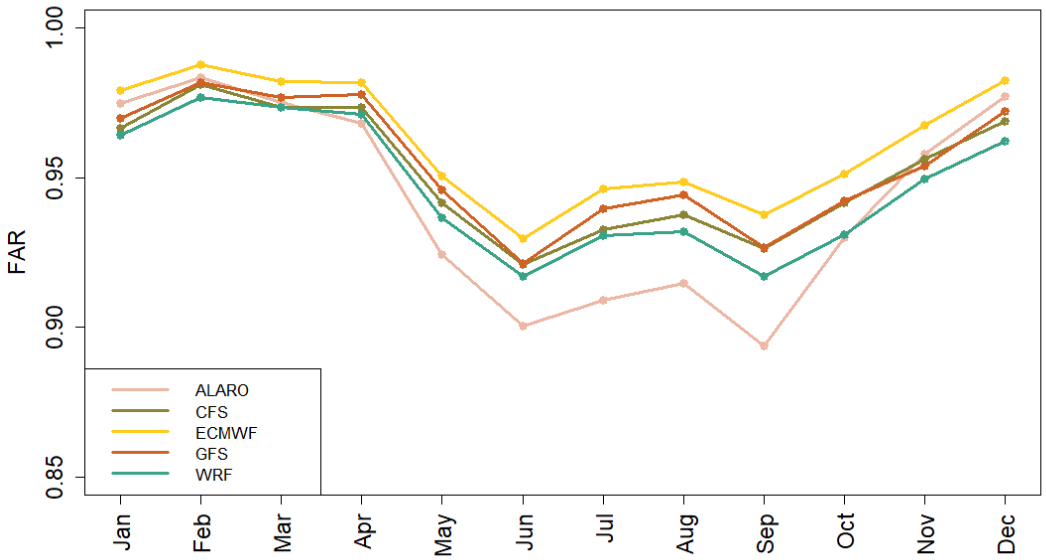

Figure 3.33. Monthly average FAR values of convective precipitation in the entire area

It has been observed that the monthly FAR values of the large-scale precipitation are similar to the total precipitation (Figure 3.34), but the models follow more discrete trends from each other. There is a rapid increase from June to July due to the increased convective precipitation. GFS product gives to best (<0.4) and CFS gives the worst (>0.4) FAR values in this precipitation component.

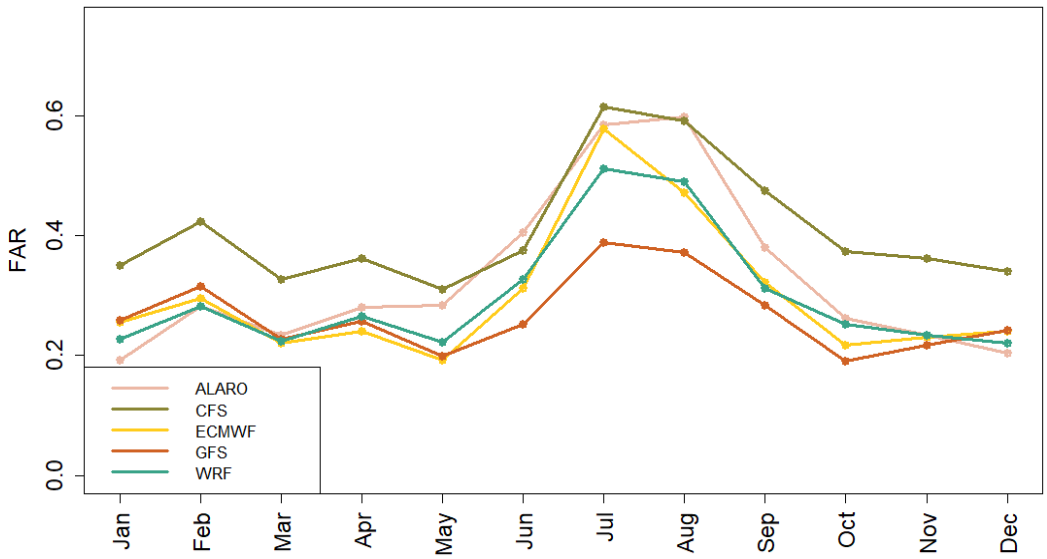

Figure 3.34. Monthly average FAR values of large-scale precipitation in the entire area

3.2.6 Seasonal Scale

3.2.6.1 Spatial Distributions

The seasonal precipitation variation in our country directly affects many areas, from agriculture to tourism, transportation to energy (Luo et al., 2007). In general, it is deduced that there is less precipitation in summers and more precipitation in winters in Turkey, so the distribution of precipitation varies from different seasonal and regional scales. For instance, while the precipitation in the winter season of 2020 is 233.5 mm, this amount decreased to 65.7 mm in the summer season (TSMS, 2020). This study shows the seasons' spatial distributions and accuracy statistics for the 3 precipitation types (total, convective, stratiform) below.

In Turkey, where the Mediterranean climate is generally prevailing, the region that receives the most precipitation in autumn is the Eastern Black Sea region. The Eastern Black Sea region receives much precipitation compared to others. It is a rainy

region in all seasons of the year and shows a significant spatial distribution difference (Figure 3.35). Disasters such as floods overflows and landslides, which are common problems today, occur on the eastern and western Black Sea coasts with the blocking of the fronts and the increase in daily precipitation intensity. This once again increases the importance of seasonal spatial distribution analyses. As can be seen in Figure 3.35, all products, except GFS, managed to catch the heavy rainfall in the Eastern Black Sea Region. In other regions, it can be deduced that the Mediterranean Region and the western Black Sea region are also rainy in autumn and that the models that best capture this situation are ALARO, WRF, and ECMWF HRES (Figure 3.35(b), Figure 3.35(c), Figure 3.35(f)). CFS product overestimated the observed precipitation in our country (Figure 3.36(e)). When the stratiform and convective precipitations are evaluated in autumn, it seems that the models that best capture the stratiform precipitation distribution are ALARO, WRF and ECMWF HRES (Figure 3.36(b), Figure 3.36(c), Figure 3.36(f) on the right side). With the cooling of the air towards winter, the convection decreases and rapid and heavy precipitation begins to be seen less frequently. It is observed slightly east of the Black Sea and on the Mediterranean coasts (Figure 3.36). This is because the mountains in these regions are parallel to the sea and the heated air rises rapidly with the effect of humidity. Although all products overestimate convective precipitation distributions, it can be said that the WRF product has the closest distribution to the observation (Figure 3.36(c) on the left side).

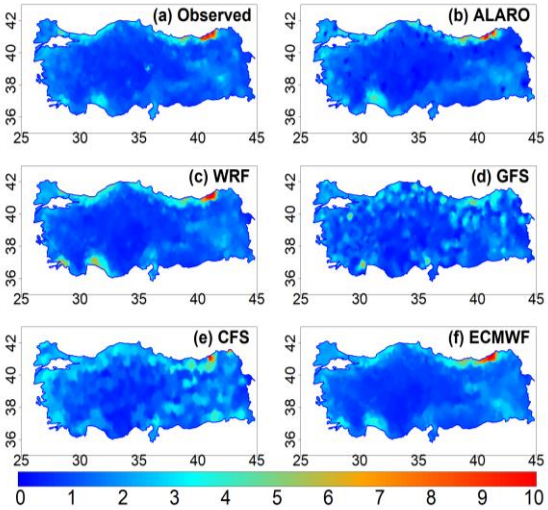

Figure 3.35. Spatial distributions of daily total precipitation (mm/day) in autumn season

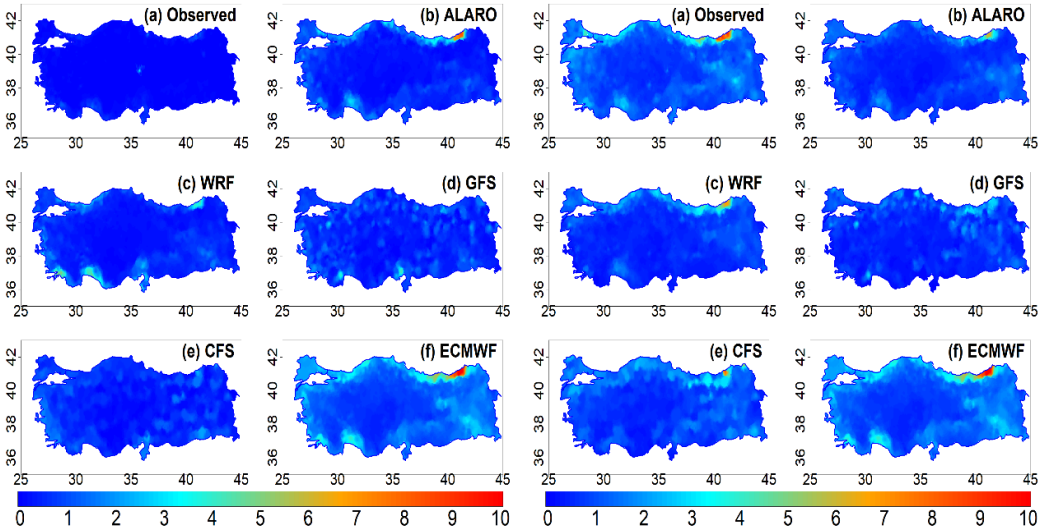

Figure 3.36. Spatial distributions of daily convective (left) and stratiform (right) precipitations (mm/day) in autumn season

The places with the highest total precipitation in Turkey during the winter months can be listed as the Menteşe Region in the Aegean, the Mediterranean coastline, the Southeastern Taurus Mountains and the Eastern Black Sea coasts. The spatial distribution of the total precipitation in Figure 3.37 shows that the models that

capture the precipitation on the Mediterranean coast are ALARO, WRF and ECMWF HRES. In addition, the products that reveal the difference in precipitation intensities in Southeast and Central Anatolia with the sharp change of colors can be interpreted as WRF and ECMWF HRES.

Stratiform precipitation affects large areas due to the meeting of heat and cold air waves coming from different directions. In our country, a result of the frontal movements indicates its effect, especially in the regions where the Mediterranean climate is dominant, starting from the Mediterranean coasts and towards the southeast during the winter months. In these regions, which receive annual average precipitation of 660 mm (TSMS, 2021), more precipitation is seen compared to the Eastern Black Sea Region due to the hot and humid weather. As seen in Figure 3.38 (right side), stratiform precipitation in the winter season starts from the Mediterranean coast and extends towards the Southeastern Anatolia Region. The product that best captures the spatial distribution of stratiform precipitation for the winter season is WRF (Figure 3.38(c)). In contrast, the second and third products that best capture the spatial distribution are ECMWF and ALARO (Figure 3.38(f), Figure 3.38(b)). In other products, although there is a rather dispersed distribution, it is seen that there is both excessive precipitation and stratiform precipitation in very different regions from the observation.

Fronts in Turkey have the most activity in winter. For this reason, most of the total precipitation belongs to stratiform precipitation in winter. As seen in Figure 3.38 (left side), convective precipitation distribution is not transparent in the observation and the product. ALARO, ECMWF and WRF showed similar distributions and revealed convective precipitation distributions more clearly.

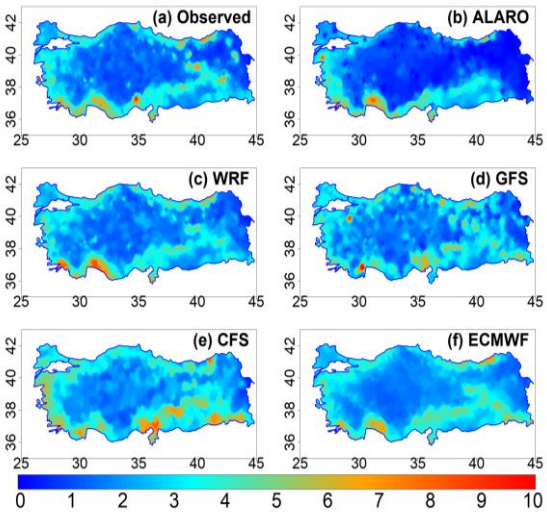

Figure 3.37. Spatial distributions of daily total precipitation (mm/day) in winter season

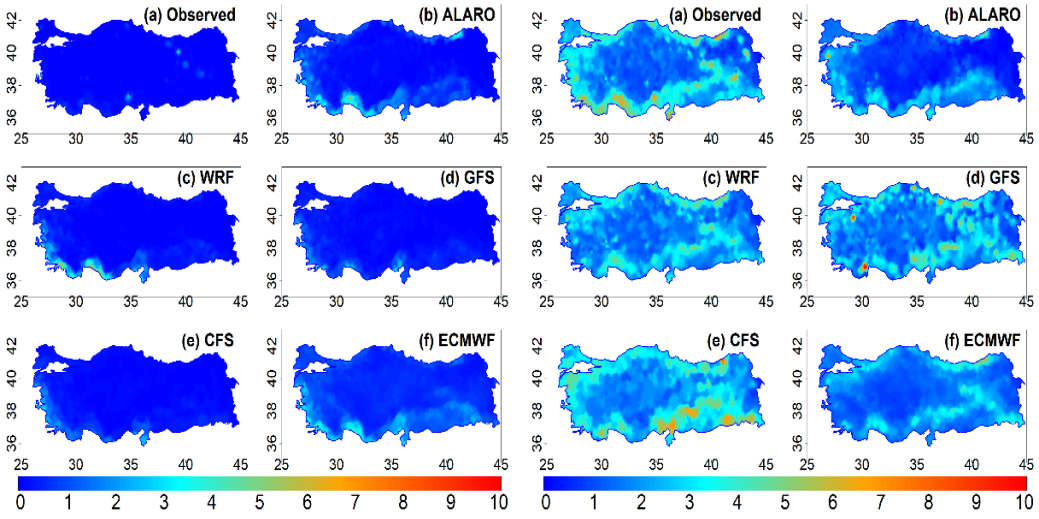

Figure 3.38. Spatial distributions of daily convective (left) and stratiform (right) precipitations (mm/day) in winter season

With the spring season, significant changes begin to occur in our country in terms of both precipitation and temperature. In the winter months, the total precipitation decreases in the coastal areas where precipitation is intense, and precipitation increases in Anatolia's inner parts. One of the most apparent changes is the

precipitation intensity in the Iğdır, Erzurum-Kars-Ardahan plateau in Northeastern Anatolia, as seen in Figure 3.39(a). Those who follow this change in products most closely are seen as GFS and CFS. However, considering that they overestimate the distribution of those products over the whole of Turkey, it can be concluded that the forecast performances of the products in the spring season are not very successful.

When the distribution of stratiform precipitation across the country is examined, it can be observed in Figure 3.40(a) (right side) that there is a significant density in Northeast Anatolia. None of the products are successful in catching this density, and when the general distributions are examined, it can be said that the product closest to the observation is WRF.

Convective precipitation, also called showers, is short-term, high-intensity precipitation. They occur when the air is saturated with moisture as the warm air rises. This results in increased precipitation in the spring and summer months. Prediction phases are challenging as they are short-term precipitations. As seen in Figure 3.40 (left side), there is no consistent distribution between observations and models.

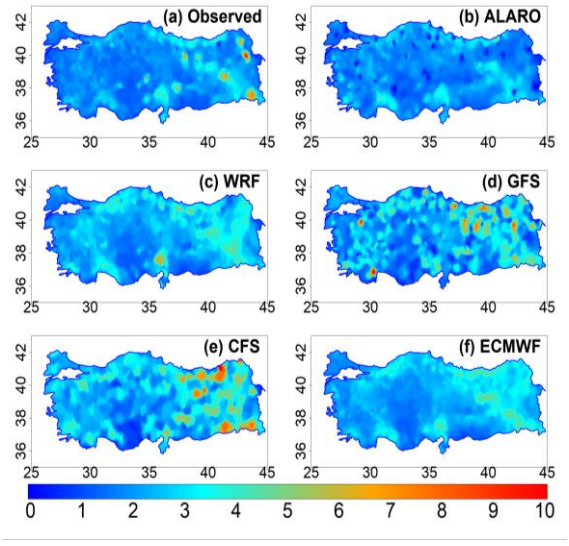

Figure 3.39. Spatial distributions of daily total precipitation (mm/day) in spring season

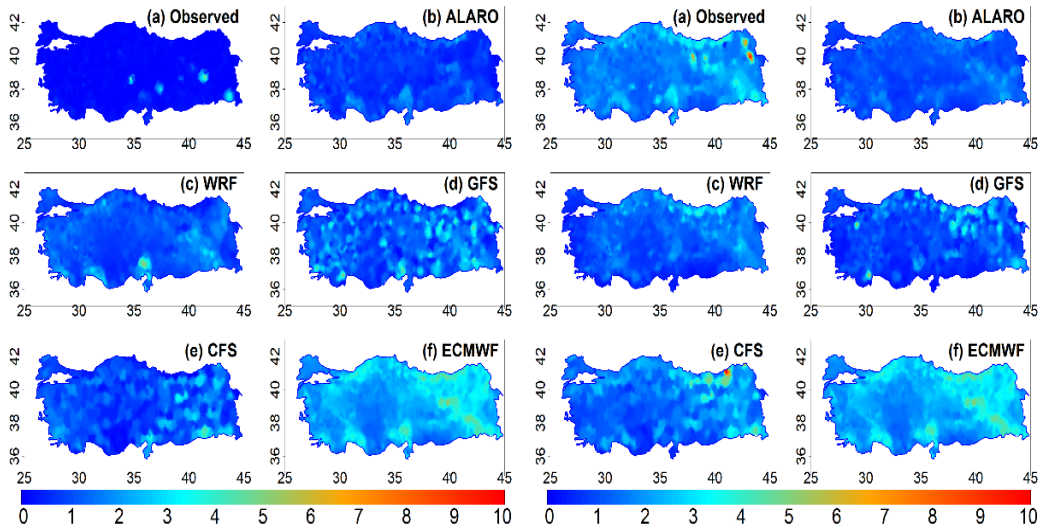

Figure 3.40. Spatial distributions of daily convective (left) and stratiform (right) precipitations (mm/day) in spring season

On the other hand, summer months are the months with the least precipitation in the country. With the dominance of tropical pressure, precipitation due to convection occurs in the northeast part of the country. While most of the total precipitation is seen especially in the Eastern Black Sea Region during the summer (Figure 3.41(a)), the most striking feature of the summer season in our country is the drought prevailing in other parts of Anatolia apart from this region. The product that captures this difference closest to the observation in total precipitation is the ECMWF HRES (Figure 3.41(f)).

In stratiform precipitation distributions, all products, except GFS, give convenient results considering the color grading (Figure 3.42 (right side)). Although convective precipitation dominates in summer with the warming of the air, contrary to the stratiform precipitation forecasts, all products failed to catch the observation since they all overestimated. While the closest ECMWF HRES and ALARO are observed in terms of catching the precipitation in near-coastal regions (Figure 3.42(b), Figure 3.42(f) (left side)), these two products did not achieve a successful result by showing the intensity of precipitation much higher than the observation.

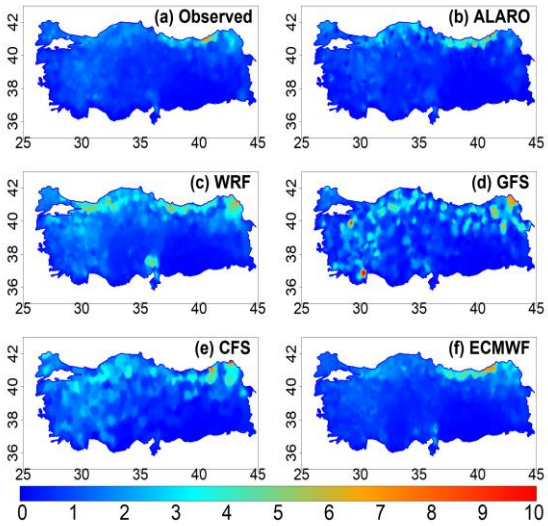

Figure 3.41. Spatial distributions of daily total precipitation (mm/day) in summer season

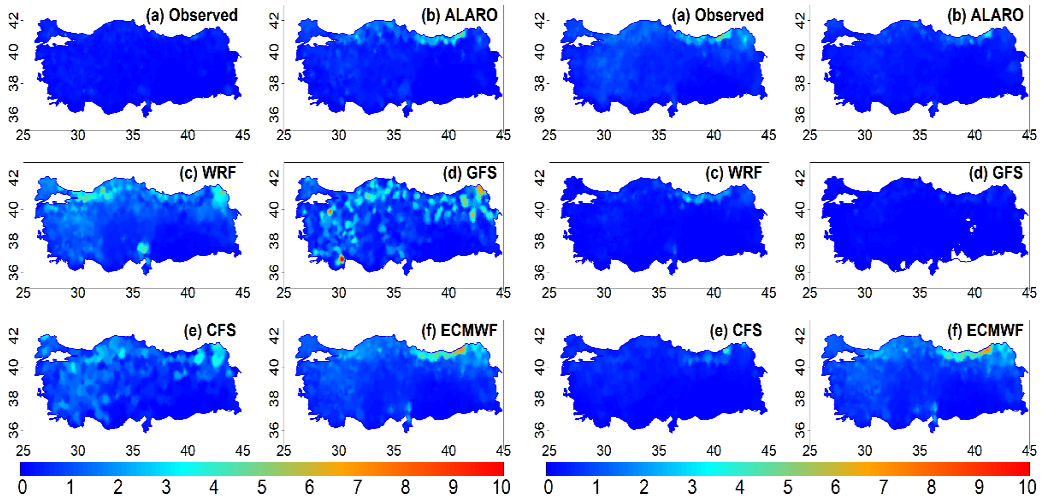

Figure 3.42. Spatial distributions of daily convective (left) and stratiform (right) precipitations (mm/day) in summer season

3.2.6.2 Accuracy Statistics

When the total daily precipitation is analyzed according to the seasons, the lowest deviation, closest mean and best bias belong to the ALARO product for all seasons (Table 3.8 and Table 3.9). Although all models have close results, the lowest error values (ErrSD and RMSE) belong to ECMWF HRES for all seasons (Table 3.9).

When the correlations are examined (Table 3.10), the products are more successful in colder months. The reason may be that the precipitation in the summer months is in the form of showers, and the models need help catching these precipitations that start and end quickly. The most successful model for CC values is ECMWF HRES as well.

Table 3.8. Mean and standard deviation values of daily total precipitation according to seasons

Precipitation Type (mm)		**TP**			
	Dataset	**Autumn**	**Winter**	**Spring**	**Summer**
Mean (mm/day)	**Observation**	1.57	2.6	2.04	0.99
	ALARO	1.55	1.97	1.97	0.9
	CFS	1.82	3.24	2.82	1.29
	ECMWF	1.7	2.85	2.49	1.04
	GFS	1.49	2.68	2.44	1.17
	WRF	1.67	2.75	2.46	1.49
Standard Deviation (mm/gün)	**Observation**	5.3	6.38	5.37	3.69
	ALARO	5.07	4.76	4.83	2.91
	CFS	4.99	6.46	5.3	3.18
	ECMWF	4.69	5.69	4.46	2.54
	GFS	4.61	5.85	4.61	2.75
	WRF	5.19	6.32	5.19	3.97

Table 3.9. Bias, RMSE and ErrSD values of daily total precipitation according to seasons

Precipitation Type (mm)		**TP**			
	Dataset	**Autumn**	**Winter**	**Spring**	**Summer**
Bias (mm/day)	**ALARO**	-0.02	-0.63	-0.07	-0.09
	CFS	0.24	0.64	0.78	0.29
	ECMWF	0.13	0.26	0.45	0.05
	GFS	-0.09	0.08	0.41	0.17
	WRF	0.1	0.16	0.43	0.5
ErrSD (mm/day)	**ALARO**	4.5	5.02	4.87	4
	CFS	4.64	5.15	5.25	4.12
	ECMWF	4	4.36	4.33	3.52
	GFS	4.55	4.69	4.98	4.06
	WRF	4.41	4.77	4.85	4.36
RMSE (mm/day)	**ALARO**	4.52	5.13	4.91	4.03
	CFS	4.74	5.33	5.44	4.21
	ECMWF	4.02	4.44	4.39	3.54
	GFS	4.64	4.83	5.13	4.18
	WRF	4.43	4.82	4.91	4.42

Table 3.10. CC and SNR values of daily total precipitation according to seasons

Precipitation Type (mm)		**TP**			
	Dataset	**Autumn**	**Winter**	**Spring**	**Summer**
CC with the observation	**ALARO**	0.66	0.63	0.60	0.37
	CFS	0.64	0.72	0.58	0.34
	ECMWF	0.71	0.77	0.66	0.41
	GFS	0.64	0.74	0.59	0.35
	WRF	0.68	0.74	0.62	0.39
SNR with the observation	**ALARO**	2.11	2.00	1.64	0.51
	CFS	1.84	2.60	1.41	0.54
	ECMWF	2.49	3.63	2.07	0.70
	GFS	1.69	2.81	1.39	0.45
	WRF	2.25	3.18	1.74	0.66

In the statistics of the convective component of precipitation, it can be inferred that the products have difficulty catching the observation since, in Table 3.11, the products showed values far from the mean and standard deviations of the observation. At the same time, the high error values in Table 3.12 reveal that the performance of the models could be better. Although the small number of data in the reference dataset significantly affects the low values, the data also dramatically affects the best CC values in the autumn season (Table 3.13). In the CC values, the WRF product is more successful in partially convective precipitation predictions than the others in all seasons.

Table 3.11. Mean and standard deviation values of daily convective precipitation according to seasons

Precipitation Type (mm)		**CP**			
	Dataset	**Autumn**	**Winter**	**Spring**	**Summer**
Mean (mm/day)	**Observation**	0.15	0.09	0.15	0.24
	ALARO	0.82	0.69	0.9	0.57
	CFS	0.69	0.38	1.13	0.94
	ECMWF	0.88	1.01	1.62	0.76
	GFS	0.74	0.41	1.36	1.06
	WRF	0.74	0.46	1.18	1.21
Standard Deviation (mm/day)	**Observation**	1.31	0.75	1.45	1.82
	ALARO	2.87	1.93	2.55	2.05
	CFS	2.12	1.1	2.4	2.26
	ECMWF	2.5	2.24	2.93	1.87
	GFS	2.34	1.21	3	2.53
	WRF	2.8	1.45	3	3.33

Table 3.12. Bias, RMSE and ErrSD values of daily convective precipitation according to seasons

Precipitation Type (mm)		**CP**			
	Dataset	**Autumn**	**Winter**	**Spring**	**Summer**
Bias (mm/day)	**ALARO**	0.67	0.6	0.76	0.33
	CFS	0.54	0.29	0.98	0.7
	ECMWF	0.73	0.92	1.48	0.52
	GFS	0.59	0.32	1.22	0.82
	WRF	0.6	0.38	1.04	0.97
ErrSD (mm/day)	**ALARO**	2.96	2.23	3.08	2.66
	CFS	2.4	1.47	2.94	2.84
	ECMWF	2.64	2.49	3.34	2.44
	GFS	2.6	1.46	3.5	3.11
	WRF	2.83	1.79	3.42	3.55
RMSE (mm/day)	**ALARO**	3.05	2.34	3.19	2.7
	CFS	2.47	1.53	3.15	2.97
	ECMWF	2.75	2.69	3.71	2.51
	GFS	2.68	1.52	3.76	3.27
	WRF	2.89	1.85	3.61	3.7

Table 3.13. CC and SNR values of daily convective precipitation according to seasons

Precipitation Type (mm)		**CP**			
	Dataset	**Autumn**	**Winter**	**Spring**	**Summer**
CC with the observation	**ALARO**	0.21	0.13	0.15	0.15
	CFS	0.23	0.14	0.19	0.19
	ECMWF	0.25	0.15	0.17	0.2
	GFS	0.24	0.14	0.17	0.18
	WRF	0.27	0.15	0.2	0.21
SNR with the observation	**ALARO**	0.23	0.09	0.13	1.62
	CFS	0.26	0.14	0.17	2.16
	ECMWF	0.26	0.10	0.13	1.65
	GFS	0.25	0.13	0.13	2.48
	WRF	0.30	0.12	0.15	3.01

The seasonal statistics of stratiform precipitation in our country show that the slightest deviation from the observation belongs to the CFS model (Table 3.14). The slightest error values in all seasons belong to ECMWF HRES and ALARO (Table 3.15). As expected, the CC values of the stratiform precipitations, which are most prominent in the winter, are pretty high compared to other seasons. CFS, which stands out again in signal-noise ratios, has values close to ALARO and ECMWF HRES products in CC values (Table 3.16) and can be called the most successful product in stratiform precipitation.

Table 3.14. Mean and standard deviation values of daily large-scale precipitation according to seasons

Precipitation Type (mm)		**LSP**			
	Dataset	**Autumn**	**Winter**	**Spring**	**Summer**
Mean (mm/day)	**Observation**	1.43	2.51	1.9	0.75
	ALARO	0.9	1.39	1.17	0.37
	CFS	1.13	2.86	1.69	0.35
	ECMWF	0.82	1.84	0.86	0.28
	GFS	0.75	2.27	1.08	0.11
	WRF	0.93	2.29	1.28	0.28
Standard Deviation (mm/day)	**Observation**	4.6	5.98	2.58	2.44
	ALARO	2.95	3.43	2.99	1.18
	CFS	3.85	5.91	4.15	1.64
	ECMWF	2.83	4.19	2.33	0.97
	GFS	3.21	5.35	3.07	0.66
	WRF	3.55	5.58	3.56	1.27

Table 3.15. Bias, ErrSD and RMSE values of daily large-scale precipitation according to seasons

Precipitation Type (mm)		**LSP**			
	Dataset	**Autumn**	**Winter**	**Spring**	**Summer**
Bias (mm/day)	**ALARO**	-0.52	-1.12	-0.72	-0.37
	CFS	-0.3	0.35	-0.21	-0.4
	ECMWF	-0.6	-0.67	-1.03	-0.47
	GFS	-0.68	-0.24	-0.81	-0.64
	WRF	-0.5	-0.22	-0.61	-0.47
ErrSD (mm/day)	**ALARO**	3.45	4.59	3.61	2.25
	CFS	3.87	4.71	4.25	2.63
	ECMWF	3.42	4.14	3.67	2.31
	GFS	3.87	4.46	3.96	2.39
	WRF	3.69	4.45	3.81	2.49
RMSE (mm/day)	**ALARO**	3.51	4.75	3.69	2.29
	CFS	3.93	4.86	4.32	2.68
	ECMWF	3.48	4.25	3.82	2.37
	GFS	3.96	4.61	4.09	2.48
	WRF	3.74	4.52	3.87	2.55

Table 3.16. CC and SNR values of daily large-scale precipitation according to seasons

Precipitation Type (mm)		LSP			
	Dataset	**Autumn**	**Winter**	**Spring**	**Summer**
CC with the observation	**ALARO**	0.69	0.62	0.29	0.39
	CFS	0.63	0.71	0.61	0.26
	ECMWF	0.67	0.74	0.4	0.33
	GFS	0.62	0.72	0.36	0.22
	WRF	0.65	0.73	0.6	0.27
SNR with the observation	**ALARO**	1.84	1.49	1.45	0.46
	CFS	1.73	2.52	1.28	0.32
	ECMWF	1.66	2.63	1.09	0.30
	GFS	1.39	2.55	1.09	0.14
	WRF	1.83	2.84	1.47	0.29

3.2.6.3 Correlation Maps

Spatially distributed daily correlation coefficient maps are illustrated in Figure 3.43 with a resolution of 0.5°. This process is performed using inverse weighted distance interpolation. In other words, closest 3 stations are selected in the specified grid and their weighted averages are calculated proportional with their distances. Results show that CC are very similar between TP and LSP distributions. Moreover, it can be deduced that ECMWF HRES is the best performer in these two precipitation types, since it shows a darker coloring in more areas. In CP distributions, the CC values are quiet smaller than other precipitation types. However, the WRF product shows a slightly higher CC distribution among others. All model products show a moderately higher correlations in mediterranean costs. The worst performer in CP is

GFS product, as it has the lowest CC values in the entire area. These distributions are also supporting the accuracy statistics, since they have paralell results.

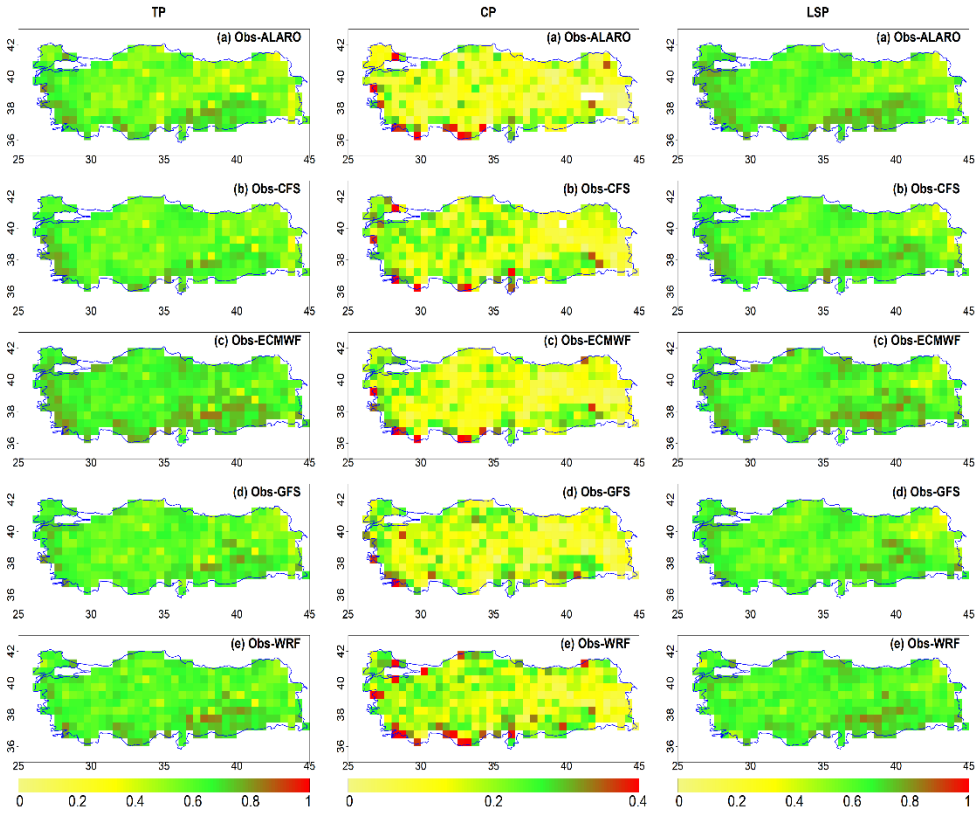

Figure 3.43. Daily spatial correlation maps for each precipitation type

3.2.7 Annual Scale

3.2.7.1 Spatial Distribution Maps

The spatial distribution of annual mean precipitation is shown in Figure 3.43 and Figure 3.44 for the observation and model-based products. The maps are obtained by equating the resolutions of each dataset at 0.05°. This process is performed using inverse weighted distance interpolation. In detail, the closest 3 stations are obtained and their influences are taken into account in direct proportion to their distance while obtaining the given resolution grid values. In other words, point form datasets are

converted to gridded form. First, when looking at the total precipitation maps, it is observed that the ALARO product (Figure 3.43 (b)) captures the observed annual precipitation better than other models, while the distribution of ECMWF HRES is the second best one, showing rather close but excessive precipitation. For example, the Eastern Black Sea region of our country has a very high precipitation rate (approximately 820-2300 mm/year, (TSMS, 2018)) and Central Anatolia is one of the regions receiving the least precipitation (approximately 400-500 mm/year, (TSMS, 2020)), this difference is reflected in the Figure 3.43 (a). The models that best capture this transition are observed primarily as ALARO and ECMWF HRES. After these two models, it can be interpreted that the WRF product has the highest performance since it captures the color transitions better (Figure 3.43 (c)). However, in this product's west side of the Black Sea, it can be observed that the WRF product overestimated the existing amount. On the other hand, CFS and GFS underperformed (Figure 3.43 (d), Figure 3.43 (e)) and could not capture the distribution very well.

While a clear distribution could not be observed in the spatial distribution of the observed convective precipitation (Figure 3.44, right side), there needs to be a more consistent distribution among the models. Considering that tonvective precipitation is more intense in humid and warm regions in our country; ECMWF HRES (Figure 3.44 (f), right side) shows this precipitation distribution on the Mediterranean coasts, especially ALARO and WRF (Figure 3.44 (b), Figure 3.44 (c), right side) show a consistent distribution as well. Moreover, the ALARO product shows a very high convective precipitation distribution in the Eastern Black Sea, which is relatable with convective precipitation conditions. GFS and CFS (Figure 3.44 (d), Figure 3.44 (e) right side) products visualized the worst distribution; they reflect an uneven spatial distribution for convective precipitation.

Although almost every product has caught the heavy stratiform precipitation in the east of the Black Sea, there is a similar underestimation in ALARO and ECMWF HRES products across the country (Figure 3.44 (b), Figure 3.44 (e), left side). The Mediterranean coast and the northeastern part of our country have high-density

precipitation in observation (Figure 3.44 (a), left side) that is catched by all products except GFS. Overall, GFS is the worst performer due to its messy illustration.

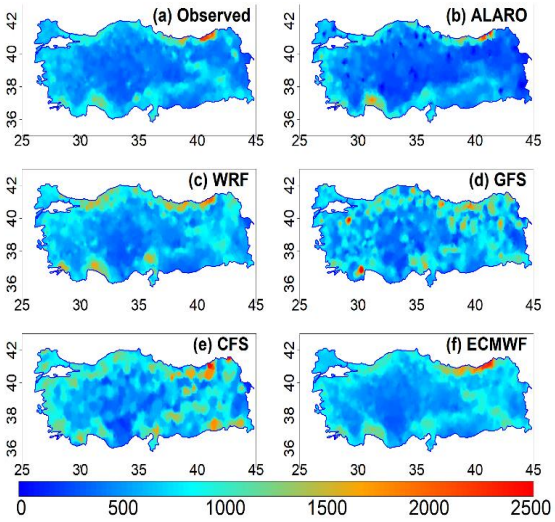

Figure 3.44. Annual spatial distribution of total precipitation (mm/year)

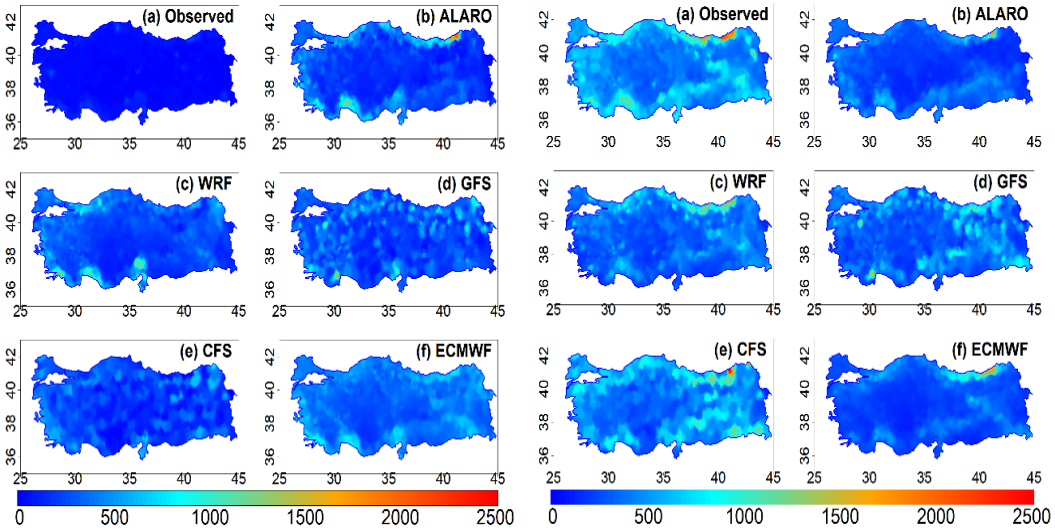

Figure 3.45. Annual spatial distributions of convective (left side) and stratiform (right side) precipitations (mm/year)

The spatial distributions of five products are shown in Figure 3.45. Although ALARO (Figure 3.45 (a)), ECMWF HRES (Figure 3.45 (c)) and WRF (Figure 3.45)) show a smooth transitions between regions, other two products show a sharper

transitions due to their coarser resolutions. High-intensity precipitation in the eastern Black Sea and Mediterranean coasts is captured in these three high-resolution model products. CFS and GFS products are underperformed due to their lower resolutions.

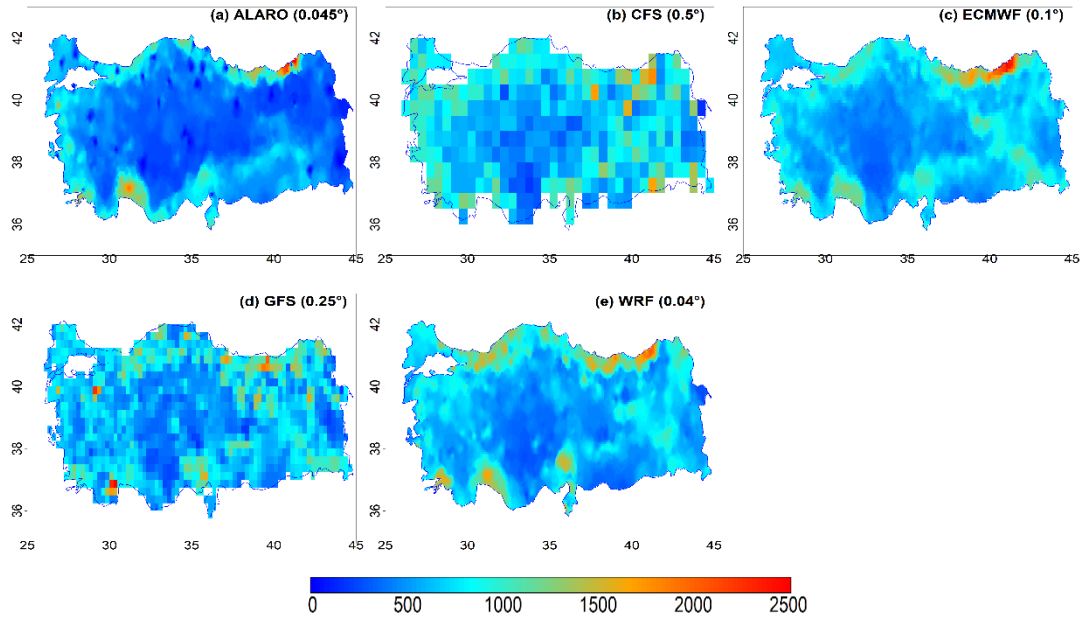

Figure 3.46. Spatial distribution maps of annual mean precipitation at the resolutions of the model datasets (mm/year)

Table 3.17 shows the spatial correlation coefficients of existing model datasets. It can be deduced that ALARO is the most successful product for TP, CP and LSP. ECMWF HRES and WRF products are also good performers while CFS and GFS products lower performed. The results are consistent with products' resolutions.

	Dataset	TP	CP	LSP
CC with the observation	ALARO	0.887	0.816	0.880
	CFS	0.465	0.372	0.543
	ECMWF	0.882	0.689	0.857
	GFS	0.418	0.311	0.533
	WRF	0.827	0.714	0.799

Table 3.17. Annual spatial correlation coefficients of model products

CHAPTER 4

SUMMARY, CONCLUSION, AND RECOMMENDATION

This study investigates the prediction performance of precipitation components (total, convective, stratiform) of 5 different NWP models (ALARO, CFS, ECMWF HRES, GFS, WRF) with 836 ground-based stations as a reference on a variable topography over four (2015-2018) and six years (2015-2020) for daily and hourly scales, respectively. The topographical difference is separated in line with the study (Amjad. 2020) which sets a 5% limit on the slope. 205 stations are classified as complex and 631 stations as non-complex. Evaluations are carried out for all precipitation components separately for the entire area, complex and non-complex zones in daily scale and in hourly scale. In addition to the mean, standard deviation, bias, error standard deviation, correlation coefficient and signal-to-noise ratio values; CPI statistics, intensity-frequency analyses and spatial distribution maps are also obtained on a daily time scale. The monthly time series of precipitation datasets and monthly average FAR values are investigated for the convective precipitation. The main outcomes are:

- Prediction performances of NWP models in hourly time scale are similar in each precipitation type.
- While the ECMWF HRES has the largest CC values for large-scale and total precipitation in all regions, the WRF product has a relatively higher CC in all regions for convective precipitation.
- In both topographical type, the CFS product has the highest ErrSD values in total and large-scale precipitation while it has the lowest ErrSD values in convective precipitation.

- According to the CPI values, it can be deduced that the ALARO product can be useful in dry day estimations in total and large-scale precipitation in complex areas. High POD and FAR values show that all products fail to catch the absence of convective precipitation. However, all products, particularly the ECMWF HRES, have a skill to detect high intensity precipitation.
- In the daily histograms of precipitation, almost all the products in total and large-scale precipitations are found to be close to the observation but the WRF product barely succeeds. While in convective precipitation distributions, although all the products are consistent among themselves, they have dramatically higher distributions than the observation.
- In the monthly distributions; all products overestimated the total and convective precipitations, underestimated the large-sale precipitation.

Overall, when the evaluations are examined, the forecast performances of the products in total precipitation and large-scale precipitation are pretty successful in all complex and non-complex areas. In this study, gridded data are converted to the closest point data and made comparable to the reference data. For this reason, catching precipitation, especially in small areas with short durations such as convective precipitation, is quite tricky, directly depending on model-based product resolution since some model products have a coarser resolution (e.g., 0.5° for CFS). Another direct effect is the measurement accuracy, number and distribution of ground observation stations that are also related to topographical features. Since convective precipitations are challenging to catch in the prediction due to rapid and heavy precipitation, model performances decrease compared to other precipitation, especially in poorly measured regions. In this context, the fact that topography has a great impact cannot be ignored. Especially the inadequacy of the number of ground observation stations in complex areas compared to non-complex areas and the decrease in measurement capabilities directly affect the accuracy analysis results. This also implies that model performances should be improved to perform more sensitive predictions due to the difficulty of making station-based observations for convective precipitations. Additionally, the limit values used in this study have an

impact while classifying the topographical type and precipitation seggregation. All results show the dependability of threshold values when determining the convective precipitation amount in the station-based dataset and number of complex and non-complex stations. Reflectivity and rainfall intensity relationships may be useful to define a more accurate threshold by using drop size distributions obtained from consistent disdrometer measurements for the future studies.

Today, floods and other disasters caused by excessive precipitation affect the regions in many ways; such as the economy, society, or industry. In our world, which is getting warmer every day, the possibility of rapid and heavy precipitation is increasing. According to the results of this study, precipitation accuracy analysis studies in both complex and flat areas should be developed and diversified with more available and comparable data in future studies.

REFERENCES

Akinyemi, D.F., Ayanlade, O.S., Nwaezeigwe, J.O., Ayanlade, A., 2020. A comparison of the accuracy of multi-satellite precipitation estimation and ground meteorological records over southwestern Nigeria. Remote Sens. Earth Syst. Sci. 3, 1–12.

Aksoy, M., 2020. Evaluation of numerical weather prediction models for flash flood warnings in Turkey.

Amjad, M., Yilmaz, M.T., Yucel, I., Yilmaz, K.K., 2020. Performance evaluation of satellite-and model-based precipitation products over varying climate and complex topography. J. Hydrol. 584, 124707.

Ashrit, R., Sharma, K., Kumar, Sushant, Dube, A., Karunasagar, S., Arulalan, T., Mamgain, A., Chakraborty, P., Kumar, Sumit, Lodh, A., 2020. Prediction of the August 2018 heavy rainfall events over Kerala with high-resolution NWP models. Meteorol. Appl. 27, e1906.

Bağçaci, S.Ç., Yucel, I., Duzenli, E., Yilmaz, M.T., 2021. Intercomparison of the expected change in the temperature and the precipitation retrieved from CMIP6 and CMIP5 climate projections: A Mediterranean hot spot case, Turkey. Atmos. Res. 256, 105576.

Bližňák, V., Kašpar, M., Müller, M., Zacharov, P., 2019. Sub-daily temporal reconstruction of extreme precipitation events using NWP model simulations. Atmos. Res. 224, 65–80.

Bližňák, V., Sokol, Z., Zacharov, P., 2017. Nowcasting of deep convective clouds and heavy precipitation: Comparison study between NWP model simulation and extrapolation. Atmos. Res. 184, 24–34.

Bostan, P.A., Heuvelink, G.B.M., Akyurek, S.Z., 2012. Comparison of regression and kriging techniques for mapping the average annual precipitation of Turkey. Int. J. Appl. Earth Obs. Geoinf. 19, 115–126.

Caniaux, G., Redelsperger, J.L., Lafore, J.P., 1994. A numerical study of the stratiform region of a fast-moving squall line. Part I: General description and water and heat budgets. J. Atmos. Sci. 51, 2046–2074.

Chen, A., Chen, D., Azorin-Molina, C., 2018. Assessing reliability of precipitation data over the Mekong River Basin: A comparison of ground-based, satellite, and reanalysis datasets. Int. J. Climatol. 38, 4314–4334.

Chen, C., Hu, B., Li, Y., 2021. Easy-to-use spatial random-forest-based downscaling-calibration method for producing precipitation data with high resolution and high accuracy. Hydrol. Earth Syst. Sci. 25, 5667–5682.

Chen, H., Yong, B., Qi, W., Wu, H., Ren, L., Hong, Y., 2020. Investigating the evaluation uncertainty for satellite precipitation estimates based on two different ground precipitation observation products. J. Hydrometeorol. 21, 2595–2606.

Churchill, D.D., Houze Jr, R.A., 1984. Development and structure of winter monsoon cloud clusters on 10 December 1978. J. Atmos. Sci. 41, 933–960.

Das, S., Maitra, A., 2018. Characterization of tropical precipitation using drop size distribution and rain rate-radar reflectivity relation. Theor. Appl. Climatol. 132, 275–286.

De Troch, R., Hamdi, R., Van de Vyver, H., Geleyn, J.-F., Termonia, P., 2013. Multiscale performance of the ALARO-0 model for simulating extreme summer precipitation climatology in Belgium. J. Clim. 26, 8895–8915.

Dutton, E., Dougherty, H., 1979. Year-to-year variability of rainfall for microwave applications in the USA. IEEE Trans. Commun. 27, 829–832.

Duzenli, E., Pilatin, H., Yucel, I., Kilicarslan, B.M., Tugrul Yilmaz, M., 2020. Evaluation of the performance of WRF model in extreme precipitation estimation concerning the changing model configuration and the spatial and temporal variations, in: EGU General Assembly Conference Abstracts. p. 1026.

Duzenli, E., Yucel, I., Pilatin, H., Yilmaz, M.T., 2021. Evaluating the performance of a WRF initial and physics ensemble over Eastern Black Sea and Mediterranean regions in Turkey. Atmos. Res. 248, 105184.

European Centre for Medium-Range Weather Forecasts. (2022, November). ECMWF. Retrieved October 14, 2022, from https://www.ecmwf.int/

Edouard, S., Vincendon, B., Ducrocq, V., 2018. Ensemble-based flash-flood modelling: Taking into account hydrodynamic parameters and initial soil moisture uncertainties. J. Hydrol. 560, 480–494.

El Kenawy, A.M., Lopez-Moreno, J.I., McCabe, M.F., Vicente-Serrano, S.M., 2015. Evaluation of the TMPA-3B42 precipitation product using a high-density rain gauge network over complex terrain in northeastern Iberia. Glob. Planet. Change 133, 188–200.

Elibüyük, M., YILMAZ, E., 2010. Türkiye'nin coğrafi bölge ve bölümlerine göre yükselti basamakları ve eğim grupları. Coğrafi Bilim. Derg. 8, 27–56.

Feloni, E.G., Baltas, E.A., Nastos, P.T., Matsangouras, I.T., 2019. Implementation and evaluation of a convective/stratiform precipitation scheme in Attica region, Greece. Atmos. Res. 220, 109–119.

Foth, A., Zimmer, J., Lauermann, F., Kalesse-Los, H., 2021. Evaluation of micro rain radar-based precipitation classification algorithms to discriminate between stratiform and convective precipitation. Atmos. Meas. Tech. 14, 4565–4574.

Gaal, L., Molnar, P., Szolgay, J., 2014. Selection of intense rainfall events based on intensity thresholds and lightning data in Switzerland. Hydrol. Earth Syst. Sci. 18, 1561–1573.

Gao, W., Liu, L., Li, J., Lu, C., 2018. The microphysical properties of convective precipitation over the Tibetan Plateau by a subkilometer resolution cloud-resolving simulation. J. Geophys. Res. Atmos. 123, 3212–3227.

Ghada, W., Estrella, N., Menzel, A., 2019. Machine learning approach to classify rain type based on Thies disdrometers and cloud observations. Atmosphere (Basel). 10, 251.

Giot, O., Termonia, P., Degrauwe, D., De Troch, R., Caluwaerts, S., Smet, G., Berckmans, J., Deckmyn, A., De Cruz, L., De Meutter, P., 2015. Validation of the ALARO-0 model within the EURO-CORDEX framework. Geosci. Model Dev. Discuss. 8.

Gottardi, F., Obled, C., Gailhard, J., Paquet, E., 2012. Statistical reanalysis of precipitation fields based on ground network data and weather patterns: Application over French mountains. J. Hydrol. 432, 154–167.

Guo, X., Li, Y., Chen, X., Zhang, J., Sun, Y., 2021. Variation of debris flow/flood formation conditions at the watershed scale in the Wenchuan Earthquake area. Landslides 18, 2427–2443.

Hazra, A., Chaudhari, H.S., Dhakate, A., 2016. Evaluation of cloud properties in the NCEP CFSv2 model and its linkage with Indian summer monsoon. Theor. Appl. Climatol. 124, 31–41.

Hughes, M., Hall, A., Fovell, R.G., 2009. Blocking in areas of complex topography, and its influence on rainfall distribution. J. Atmos. Sci. 66, 508–518.

IPCC, 2014. AR5 Synthesis Report: Climate Change.

Jafarpour, M., Adib, A., Lotfirad, M., 2022. Improving the accuracy of satellite and reanalysis precipitation data by their ensemble usage. Appl. Water Sci. 12, 1–15.

Jain, S., 2015. WRF model analysis of land-surface processes over Jaipur Region. Int. J. Sci. Eng. Technol 6, 1276–1284.

Jiang, Q., Li, W., Fan, Z., He, X., Sun, W., Chen, S., Wen, J., Gao, J., Wang, J., 2021. Evaluation of the ERA5 reanalysis precipitation dataset over Chinese

Mainland. J. Hydrol. 595, 125660.

Jodar-Abellan, A., Valdes-Abellan, J., Pla, C., Gomariz-Castillo, F., 2019. Impact of land use changes on flash flood prediction using a sub-daily SWAT model in five Mediterranean ungauged watersheds (SE Spain). Sci. Total Environ. 657, 1578–1591.

Johansson, B., Chen, D., 2003. The influence of wind and topography on precipitation distribution in Sweden: Statistical analysis and modelling. Int. J. Climatol. A J. R. Meteorol. Soc. 23, 1523–1535.

Karadavut, C., 2014. Wrf Ve Alaro Sayısal Hava Tahmin Modelleri İçin Verifikasyon Sonuçlarının Karşılaştırılması.

Kidd, C., Huffman, G., 2011. Global precipitation measurement. Meteorol. Appl. 18, 334–353.

Kim, J., Park, S.K., 2016. Uncertainties in calculating precipitation climatology in East Asia. Hydrol. Earth Syst. Sci. 20, 651–658.

Kirsch, B., Clemens, M., Ament, F., 2019. Stratiform and convective radar reflectivity–rain rate relationships and their potential to improve radar rainfall estimates. J. Appl. Meteorol. Climatol. 58, 2259–2271.

Koukoula, M., Nikolopoulos, E.I., Kushta, J., Bartsotas, N.S., Kallos, G., Anagnostou, E.N., 2019. A numerical sensitivity analysis of soil moisture feedback on convective precipitation. J. Hydrometeorol. 20, 23–44.

Kyselý, J., Rulfová, Z., Farda, A., Hanel, M., 2016. Convective and stratiform precipitation characteristics in an ensemble of regional climate model simulations. Clim. Dyn. 46, 227–243.

Lei, H., Li, H., Zhao, H., Ao, T., Li, X., 2021. Comprehensive evaluation of satellite and reanalysis precipitation products over the eastern Tibetan plateau characterized by a high diversity of topographies. Atmos. Res. 259, 105661.

Li, G., Yu, Z., Wang, W., Ju, Q., Chen, X., 2021. Analysis of the spatial Distribution of precipitation and topography with GPM data in the Tibetan Plateau. Atmos. Res. 247, 105259.

Lien, G.-Y., Kalnay, E., Miyoshi, T., Huffman, G.J., 2016. Statistical properties of global precipitation in the NCEP GFS model and TMPA observations for data assimilation. Mon. Weather Rev. 144, 663–679.

Llasat, M., 2001. An objective classification of rainfall events on the basis of their convective features: application to rainfall intensity in the northeast of Spain. Int. J. Climatol. A J. R. Meteorol. Soc. 21, 1385–1400.

Llasat, M.C., Marcos, R., Turco, M., Gilabert, J., Llasat-Botija, M., 2016. Trends in flash flood events versus convective precipitation in the Mediterranean region: The case of Catalonia. J. Hydrol. 541, 24–37.

Luo, L., Wood, E.F., Pan, M., 2007. Bayesian merging of multiple climate model forecasts for seasonal hydrological predictions. J. Geophys. Res. Atmos. 112.

Mathew, M.M., Sreelash, K., Mathew, M., Arulbalaji, P., Padmalal, D., 2021. Spatiotemporal variability of rainfall and its effect on hydrological regime in a tropical monsoon-dominated domain of Western Ghats, India. J. Hydrol. Reg. Stud. 36, 100861.

McTaggart-Cowan, R., Vaillancourt, P.A., Zadra, A., Chamberland, S., Charron, M., Corvec, S., Milbrandt, J.A., Paquin-Ricard, D., Patoine, A., Roch, M., 2019. Modernization of atmospheric physics parameterization in Canadian NWP. J. Adv. Model. Earth Syst. 11, 3593–3635.

Poujol, B., Sobolowski, S.P., Mooney, P.A., Berthou, S., 2020. A physically based precipitation separation algorithm for convection-permitting models over complex topography. Q. J. R. Meteorol. Soc. 146, 748–761.

Rao, G.V., Reddy, K.V., Sridhar, V., Srinivasan, R., Umamahesh, N. V, Pratap, D., 2022. Evaluation of NCEP-GFS-based Rainfall forecasts over the Nagavali and Vamsadhara basins in India. Atmos. Res. 278, 106326.

Ren, X., Shao, A., Liu, W., Li, L., 2022. Improvements on short-term precipitation forecast in Northwest China based on regionally optimized moisture adjustment scheme for convective-scale NWP. Atmos. Res. 273, 106167.

Roberts, N., 2008. Assessing the spatial and temporal variation in the skill of precipitation forecasts from an NWP model. Meteorol. Appl. A J. Forecast. Pract. Appl. Train. Tech. Model. 15, 163–169.

Saedi, A., Saghafian, B., Moazami, S., Aminyavari, S., 2020. Performance evaluation of sub-daily ensemble precipitation forecasts. Meteorol. Appl. 27, e1872.

Saha, S., Nadiga, S., Thiaw, C., Wang, J., Wang, W., Zhang, Q., Van den Dool, H.M., Pan, H.-L., Moorthi, S., Behringer, D., 2006. The NCEP climate forecast system. J. Clim. 19, 3483–3517.

Sahlaoui, Z., Mordane, S., Wattrelot, E., Mahfouf, J., 2020. Improving heavy rainfall forecasts by assimilating surface precipitation in the convective scale model AROME: A case study of the Mediterranean event of November 4, 2017. Meteorol. Appl. 27, e1860.

Šaur, D., Kuliushina, A., Gaál, L., 2021. Radar and Station Measurement Tresholds for More Accurate Forecast of Convective Precipitation, in: 2021 International Conference on Military Technologies (ICMT). IEEE, pp. 1–7.

Seastedt, T.R., Bowman, W.D., Caine, T.N., McKnight, D., Townsend, A., Williams, M.W., 2004. The landscape continuum: a model for high-elevation ecosystems. Bioscience 54, 111–121.

Seela, B.K., Janapati, J., Lin, P., Wang, P.K., Lee, M., 2018. Raindrop size distribution characteristics of summer and winter season rainfall over north Taiwan. J. Geophys. Res. Atmos. 123, 11–602.

Sensoy, S., Demircan, M., Ulupinar, Y., Balta, I., 2008. Climate of turkey. Turkish state Meteorol. Serv. 401.

Servei Meteorològic de Catalunya - Departament d'Acció Climàtica, Alimentació i Agenda Rural

Simon, A., Belluš, M., Čatlošová, K., Derková, M., Dian, M., Imrišek, M., Kaňák, J., Méri, L., Neštiak, M., Vivoda, J., 2021. Numerical simulations of June 7, 2020 convective precipitation over Slovakia using deterministic, probabilistic, and convection-permitting approaches. Q. J. Hungarian Meteorol. Serv. 125, 571–607.

Singhal, A., Cheriyamparambil, A., Samal, N., Jha, S.K., 2022a. Relating forecast and satellite precipitation to generate future skillful ensemble forecasts over the northwest Himalayas at major avalanche and glacier sites. J. Hydrol. 128795.

Singhal, A., Jaseem, M., Jha, S.K., 2022b. Spatial connections in extreme precipitation events obtained from NWP forecasts: A complex network approach. Atmos. Res. 106538.

Sokol, Z., Brožková, R., Popová, J., Bobotová, G., Švábik, F., 2022. Evaluation of ALADIN NWP model forecasts by IR10. 8 μm and WV06. 2 μm brightness temperatures measured by the geostationary satellite Meteosat Second Generation. Atmos. Res. 265, 105920.

Špitalar, M., Gourley, J.J., Lutoff, C., Kirstetter, P.-E., Brilly, M., Carr, N., 2014. Analysis of flash flood parameters and human impacts in the US from 2006 to 2012. J. Hydrol. 519, 863–870.

Sridevi, C., Singh, K.K., Suneetha, P., Durai, V.R., Kumar, A., 2020. Rainfall forecasting skill of GFS model at T1534 and T574 resolution over India during the monsoon season. Meteorol. Atmos. Phys. 132, 35–52.

Steiner, M., Houze Jr, R.A., Yuter, S.E., 1995. Climatological characterization of three-dimensional storm structure from operational radar and rain gauge data. J. Appl. Meteorol. Climatol. 34, 1978–2007.

Talchabhadel, R., Sharma, S., Khadka, N., Hamal, K., Karki, S., Thapa, B.R., 2022. An outlook on the applicability of satellite precipitation products for monitoring

extreme precipitation events in Nepal Himalaya. Weather 77, 174–180.

Top, S., Kotova, L., De Cruz, L., Aniskevich, S., Bobylev, L., De Troch, R., Gnatiuk, N., Gobin, A., Hamdi, R., Kriegsmann, A., 2021. Evaluation of regional climate models ALARO-0 and REMO2015 at 0.22 resolution over the CORDEX Central Asia domain. Geosci. Model Dev. 14, 1267–1293.

Wang, Y., Tang, L., Chang, P.-L., Tang, Y.-S., 2021. Separation of convective and stratiform precipitation using polarimetric radar data with a support vector machine method. Atmos. Meas. Tech. 14, 185–197.

Ward, E., Buytaert, W., Peaver, L., Wheater, H., 2011. Evaluation of precipitation products over complex mountainous terrain: A water resources perspective. Adv. Water Resour. 34, 1222–1231.

Watson, A.I., Holle, R.L., 1982. The Relationship between Low-Level Convergence and Convective Precipitation in Illinois and South Florida. ILLINOIS STATE WATER SURVEY DIV URBANA.

Xu, D., Kivelson, M.G., Walker, R.J., Newell, P.T., Meng, C., 1995. Interplanetary magnetic field control of mantle precipitation and associated field-aligned currents. J. Geophys. Res. Sp. Phys. 100, 1837–1846.

Xu, W., Adler, R.F., Wang, N.-Y., 2014. Combining Satellite Infrared and Lightning Information to Estimate Warm-Season Convective and Stratiform Rainfall. J. Appl. Meteorol. Climatol. 53, 180–199.

Yang, D., Wang, W., Hong, T., 2022. A historical weather forecast dataset from the European Centre for Medium-Range Weather Forecasts (ECMWF) for energy forecasting. Sol. Energy 232, 263–274.

Yang, Z., Liu, P., Yang, Y., 2019. Convective/stratiform precipitation classification using ground-based Doppler radar data based on the K-nearest neighbor algorithm. Remote Sens. 11, 2277.

Yessad, K., 2013. Basics about ARPEGE/IFS, ALADIN and AROME in the cycle 40 of ARPEGE/IFS. Meteo-France/CNRM Tech. Notes.

Yu, C., Hu, D., Liu, M., Wang, S., Di, Y., 2020. Spatio-temporal accuracy evaluation of three high-resolution satellite precipitation products in China area. Atmos. Res. 241, 104952.

Yu, L., Zhang, Y., Yang, Y., 2020. Using high-density rain gauges to validate the accuracy of satellite precipitation products over complex terrains. Atmosphere (Basel). 11, 633.

Yucel, I., Onen, A., 2014. Evaluating a mesoscale atmosphere model and a satellite-based algorithm in estimating extreme rainfall events in northwestern Turkey. Nat. Hazards Earth Syst. Sci. 14, 611–624.

Yucel, I., Onen, A., Yilmaz, K.K., Gochis, D.J., 2015. Calibration and evaluation of a flood forecasting system: Utility of numerical weather prediction model, data assimilation and satellite-based rainfall. J. Hydrol. 523, 49–66.

Zahedi, R., Eskandarpanah, R., Akbari, M., Rezaei, N., Mazloumin, P., Farahani, O.N., 2022. Development of a New Simulation Model for the Reservoir Hydropower Generation. Water Resour. Manag. 1–16.

Zeng, Z., Wang, D., Chen, Y., 2021. An investigation of convective features and ZR relationships for a local extreme precipitation event. Atmos. Res. 250, 105372.

Zhang, A., Hu, J., Chen, S., Hu, D., Liang, Z., Huang, C., Xiao, L., Min, C., Li, H., 2019. Statistical characteristics of raindrop size distribution in the monsoon season observed in southern China. Remote Sens. 11, 432.

Zhang, L., Chen, X., Lai, R., Zhu, Z., 2022. Performance of satellite-based and reanalysis precipitation products under multi-temporal scales and extreme weather in mainland China. J. Hydrol. 605, 127389.

Zhang, Z., Tian, J., Huang, Y., Chen, X., Chen, S., Duan, Z., 2019. Hydrologic

evaluation of TRMM and GPM IMERG satellite-based precipitation in a humid basin of China. Remote Sens. 11, 431.

Zhao, P., Wang, Q.J., Wu, W., Yang, Q., 2021. Which precipitation forecasts to use? Deterministic versus coarser-resolution ensemble NWP models. Q. J. R. Meteorol. Soc. 147, 900–913.

Zhou, Q., Chen, D., Hu, Z., Chen, X., 2021. Decompositions of Taylor diagram and DISO performance criteria. Int. J. Climatol. 41, 5726–5732.